

Research Article

Pore Structure Characteristics of Tight Carbonate Reservoir in Qingxi Sag, Jiuquan Basin

Xiangye Kong ^{1,2}, Jianhui Zeng ^{1,2}, Xianfeng Tan ³, Xianglu Gao,⁴ Yu Peng,⁵ Qun Luo,⁶ Qianyou Wang ⁷, Ming Wen,⁸ Xin Wang,^{1,2} Maoyun Wang,^{1,2} and Jingling Wang⁹

¹College of Geosciences, China University of Petroleum, Beijing 102249, China

²State Key Laboratory of Petroleum Resources and Prospecting, China University of Petroleum, Beijing 102249, China

³College of Petroleum and Gas Engineering, Chongqing University of Science and Technology, Chongqing 401331, China

⁴China National Petroleum Corp Xinjiang Oil Field, Xinjiang 834000, China

⁵PetroChina Huabei Oilfield Company, Renqiu 062550, China

⁶Unconventional Natural Gas Institute, China University of Petroleum, Beijing 102249, China

⁷Department of Earth, Ocean, and Ecological Sciences, University of Liverpool, Liverpool L69 3GP, UK

⁸The Lyell Centre, Heriot-Watt University, Edinburgh EH14 4AS, UK

⁹Research & Development Center of BGP Inc., CNPC, Zhuozhou 072750, China

Correspondence should be addressed to Jianhui Zeng; zengjh@cup.edu.cn and Xianfeng Tan; xianfengtan8299@163.com

Received 9 January 2021; Accepted 24 May 2021; Published 3 September 2021

Academic Editor: Xixin Wang

Copyright © 2021 Xiangye Kong et al. Exclusive Licensee GeoScienceWorld. Distributed under a Creative Commons Attribution License (CC BY 4.0).

The Xiagou Formation is the main tight oil reservoir in Qingxi Sag of Jiuquan Basin. Given the poor physical properties and other factors restricting tight oil exploitation and production in this area, studies should focus on microscopic pore structure characteristics. In this study, a nano-CT scanner, a SEM, and an NMR were used to study the pore structure characteristics of a tight carbonate reservoir in Qingxi Sag, Jiuquan Basin. The Xiagou Formation reservoir mainly consists of gray argillaceous dolomite and dolomitic mudstone. The pore categories are mainly elliptical, irregular, intergranular, and intragranular and mostly filled with clay and carbonate cement. Pore space is small, the intergranular or organic pores are mostly separated, and pore-throat is weakly connected. The throats mostly develop with lamellar and tube bundle-like characteristics and with poor seepage ability. The pore-throats mostly span from nanometer to micrometer sizes, and pore diameters are mainly concentrated in the range of 0.01–0.1 and 1–10 μm . It is a unimodal pattern mainly composed of micropores, or a bimodal regular allocation dominated by micropores supplemented by macropores. The relationship between micropore (<0.1 μm) and macropore (>1 μm) content allocation and mean pore diameter strongly controls the permeability of reservoir rocks. When macropore content reaches more than 85%, or when pore content totals less than 3%, the permeability of a reservoir remarkably increases. At a higher ratio of the average finest throat sectional area and throat-pore of reservoir rock, the throat radius lies closer to the connecting pore radius, pore and throat connectivity improves, and reservoir seepage ability becomes stronger. Based on reservoir capacity and seepage ability, pore structures of the tight carbonate reservoirs in study area are classified into type I (small-pore–thin-throat), type II (thin-pore–thin-throat), and type III (microporous–microthroat) with rock permeability > 0.1 mD, 0.05–0.1 mD, and <0.05 mD, respectively. The type I pore structure reservoir should be regarded as an indicator of tight oil “sweet spots” reservoir in the study area.

1. Introduction

Unconventional resources including shale oil and shale gas have received great attention in the last few decades [1, 2]. Tight oil, as another kind of unconventional resources, has

become a research hotspot. Numerous scholars concentrate on tight oil reservoirs, especially on the micropore structure of reservoirs [3–6]. Tight oil refers to the oil resources in tight reservoirs such as tight sandstone, tight carbonate rock, or mixed rock with permeability less than or equal to 0.1 mD

under overburden pressure. In the Jiuquan Basin, the portion of Qingxi Sag is small but enriched in oil and contains mainly carbonate rocks and clastic rocks that are deposited in the sag. Well-developed carbonate rocks and fractured reservoirs are the main oil-producing layers in Yumen Oilfield [7–11]. The pore types are primarily composed of elliptical and irregular intergranular pores. The intercrystalline pores and organic pores are mostly isolated and have poor connectivity. On the micron scale, pore-throat sizes vary, showing a shelf shape, a band shape, and a spherical shape. On the nanoscale, we observed more nanoscale pores. These pores are conch-like and spherical on the surface or interior of mineral grains (crystals). Nanoscale spherical micropores have poor connectivity and are isolated in three-dimensional space, and most of them are reservoir spaces. The nanosized short shelf micropores are connected with the microshelf micropores, which are adjacent to the isolated spherical nanopores and act as both pore-throat and pore structures [12]. In recent years, with the in-depth exploration of Qingxi Sag and the improvement of oilfield development technologies, tight oil has become a key exploration and development resource in the region [13–16]. Liugouzhuang is located in the central part of the sag. Dolomite and mudstone developed widely with a long and consistent hydrocarbon charging history, yielding abundant oil and gas, whereas numerous tight oil reservoirs have occurred around oil and gas reservoirs in the area [17–19]. With the continuous exploration of tight reservoirs in Liugouzhuang, Qingxi Sag, Jiuquan Basin, massive geological data and useful practice experiences are accumulated; however, difficulty arises from analyzing the pore structure of the tight oil reservoir in the Xiagou Formation, and the accuracy of pore structure classification and evaluation remains low [20–25]. Therefore, this work is aimed at investigating the pore structure characteristics of the Xiagou Formation in Qingxi Sag, Jiuquan Basin, to discuss the comprehensive division and assessment methods of the pore structure in tight oil carbonate reservoirs, improving classification accuracy of “sweet spots” in the reservoir, and to provide guidance for the exploration and development of tight oil carbonate reservoirs. At the same time, the basic types, geological characteristics, resource potential, and exploration status of different types of continental tight oil in China are deeply studied, and some ideas and suggestions are put forward.

2. Geologic Setting

The Jiuquan Basin is positioned at the eastern boundary of Heli Mountain, the western border of Hongliuxia, the northern boundary of Dabei Mountain, and the southern boundary of Qilian Mountain [26, 27]. The entire basin area is approximately 2.2×10^4 km². Jiuquan Basin is divided into two depressions by the Jiayuguan Uplift [28, 29]; the east to west basin area is divided into two depressions of Jiudong and Jiuxi. The area of the Jiudong depression measures 1.1×10^4 km², whereas the Jiuxi depression features a smaller area of 0.68×10^4 km² and the three mainly sedimentary developed sags of Qingxi, Shida, and Huahai [30, 31] (Figure 1). The Qingxi Sag in the research area is positioned

in the western Jiuxi depression and features a rhombic shape distributed along the northwest direction [32]. The northern part of Qingxi Sag is the Altyn Tagh strike-slip fault, the southern part is the North Qilian thrust fault zone, and the eastern part is bounded by the 509 Fault [33–35]. The sag comprises four provenance areas, including east, south, west, and north. Three kinds of depositional systems grew in the Lower Cretaceous strata: fan delta, lake, and sublacustrine fan [36, 37]. The current area of Qingxi Sag totals 490 km². The Hongnan and Qingnan subsags and the Qingxi low sag are distributed in the sags from west to east. At present, the actually proven reserves measure 1.62×10^8 t, accounting for 76% of the total resources in the Jiuxi depression and earning the “small but fat” reputation [38, 39]. The Xiagou Formation is located in the center of the sag, where the source and the reservoir of the strata are integrated [26]. This formation not only serves as a hydrocarbon source rock in the basin but also as desirable oil and gas reservoir with a thickness of about 1000 m. Thick and gray glutenite developed at the bottom of the strata. Two kinds of lithologies are interbedded and developed in the lower part of the strata: a grayish green conglomerate and gray dolomitic mudstone [40]. The upper part of the strata features various lithologies with different thicknesses and interbedded deposits with dark mudstone, shale, dolomitic siltstone, and dolomitic mudstone. The top is occupied with gray mudstone and shale with different thicknesses and interbedded deposits. The strata developed with horizontal and trough crossing bedding [12, 41] (Figure 2).

3. Samples and Methods

3.1. Samples. Twenty core samples were collected from wells Long104, Q2-4, Liu4, and Liu102 in Qingxi Sag. All specimens were acquired from the Xiagou Formation reservoir and observed in terms of carbonate lithology. Rock types were dolomitic mudstone, argillaceous dolomite, and dolomitic siltstone. Organic matters initially comprised types I and II, and total organic carbon (TOC) was 0.5%–2.5% with a peak above 4%. Organic matter with TOC > 1.5% occupied over 50%, indicating that the TOC level was medium to high. Rocks from this formation had a Ro of 0.5% to 1.0%, implying that the majority of the source rocks are mature and are at a hydrocarbon production phase.

3.2. Methods. The MicroMR12-025V nuclear magnetic resonance (NMR) laboratory apparatus (Niumag Electronic Technology Co., Ltd.) was operated at a resonance frequency of 11.826 MHz, a magnet temperature of $32 \pm 0.02^\circ\text{C}$, and an echo interval of 0.30 ms [42, 43]. Cylinder specimens were measured to be 50 mm in length and 25 mm in diameter. The primary samples without any treatment were tested at first. Full water samples were evacuated for 4 h in a pressurized vacuum saturator and saturated under pressure for 16 h.

Using highly precise nanocomputed tomography (CT), we observed and quantified nanopore-throats of a tight reservoir [44–48]. Micro- and nanoscale CT scanning also enabled the examination and experiments of pore-throats at the two scales. Noninvasive 3D rock imaging, which facilitates identification of allocation, size, and connectivity of micro-

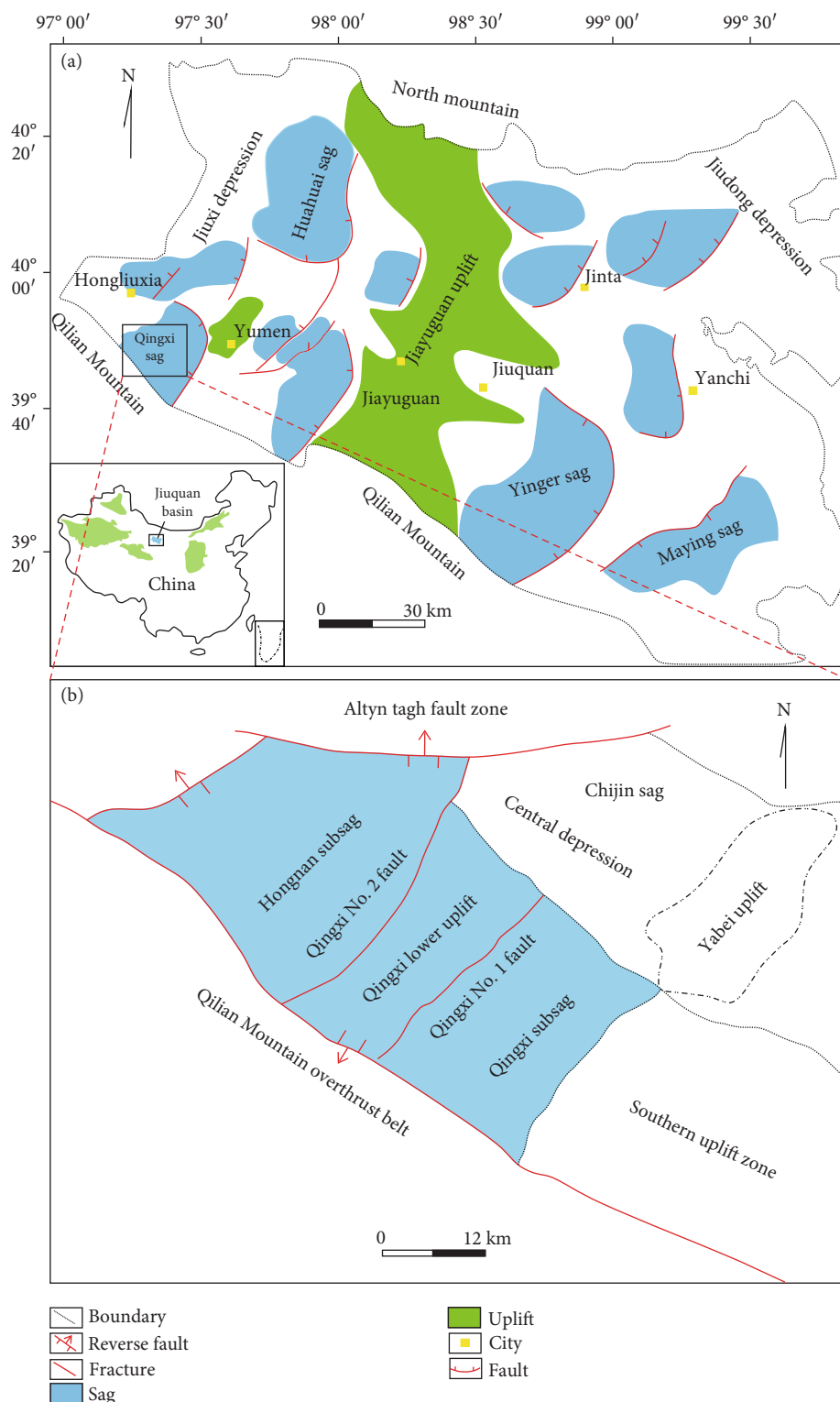


FIGURE 1: Schematic diagram of Qingxi Sag in Jiuquan Basin. (a) Map showing the location of the Qingxi Sag. (b) Outline map of the Qingxi Sag.

and nanopores, enabled the characterization of micropore- and nanopore-throat networks. Herein, nano-CT (highest resolution of 65 nm) approaches were combined. An UltraXRM-L200 nano-CT scanner from the Nanophysics Lab of the China University of Petroleum, Beijing, was employed.

A 3D pore-throat stereogram was plotted by high-resolution nano-CT scanning of 2 samples with a diameter of 65 μm .

Scanning electron microscopy (SEM) can uncover pore and interstitial features [47–50]. Rock specimens were firstly extracted and cleaned. Then, the fresh surface was processed

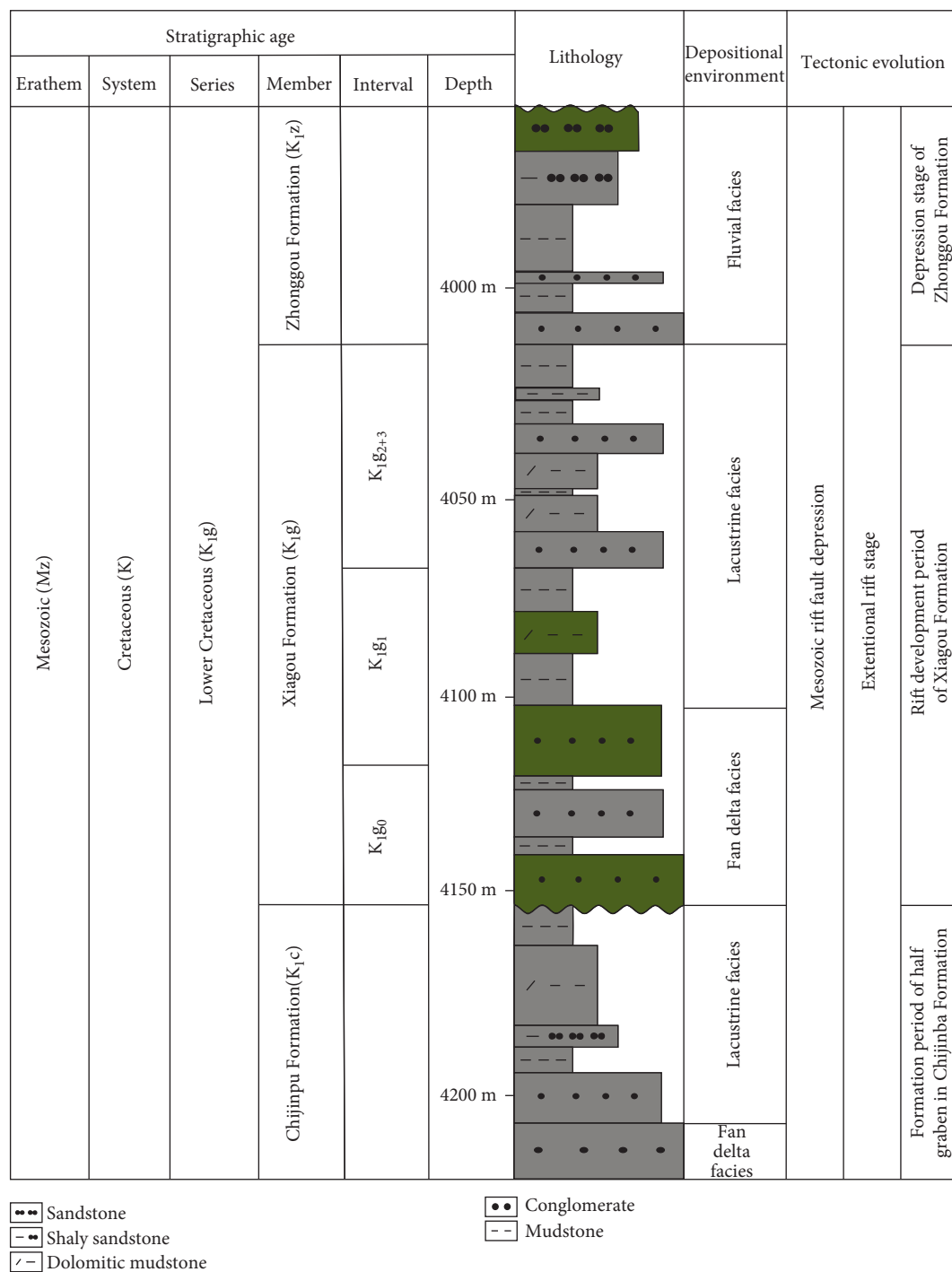


FIGURE 2: Comprehensive stratigraphic column of Lower Cretaceous strata in Qingxi Sag.

as the observation surface, and a conductive adhesive was used to fix the sample on the pile. The sample was dried naturally and finally plated with gold palladium alloy in the vacuum coating machine. Sample diameter measured 1 cm. A high-pressure mercury intrusion test was measured by a computer-controlled 9505 mercury porosimeter as per "Detection of Rock Capillary Pressure Curve" (SY/T 5346-2005). Maximum mercury pressure measured was 35 Mpa. The balancing time was set at 40 s.

4. Results

4.1. Physical Properties of Reservoir

4.1.1. *Porosity and Permeability.* The dolomitic mudstone and argillaceous dolomite that developed in the central part of Qingxi Sag are closely associated with source rocks and act as the main reservoirs of tight oil in the Xiagou Formation [50, 51]. To characterize the porosity and permeability in the

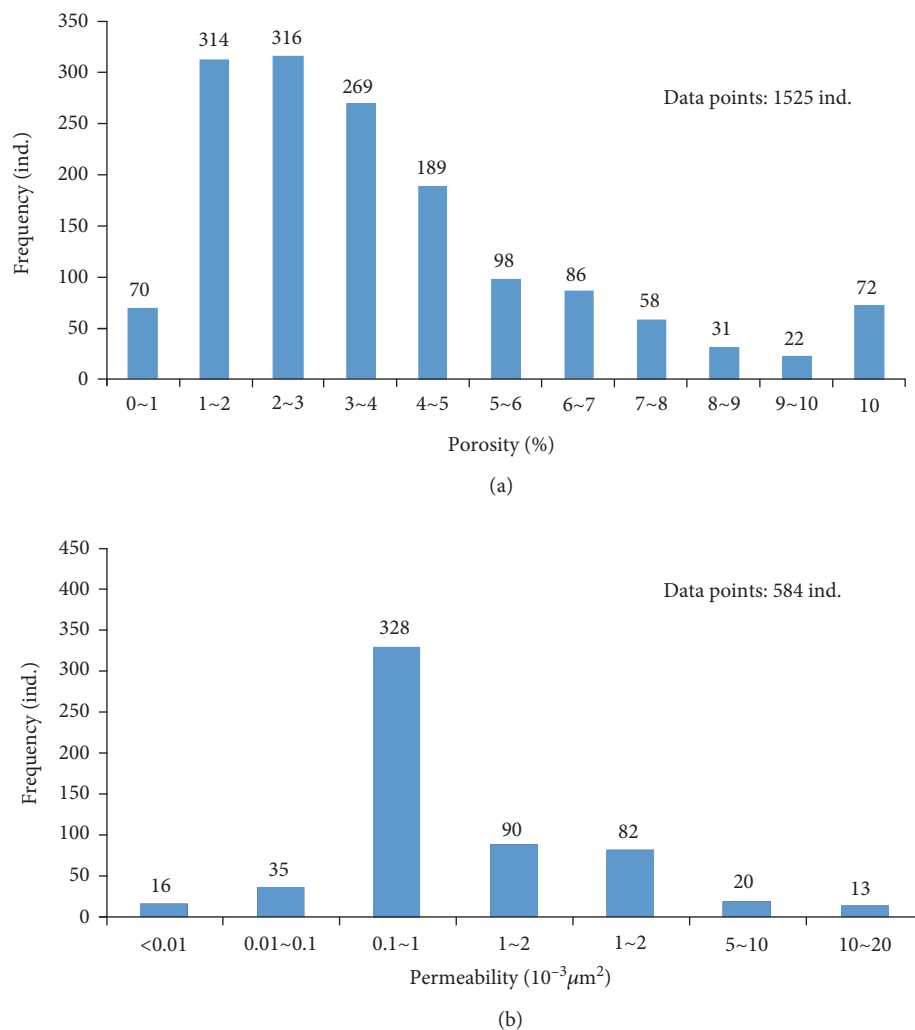


FIGURE 3: Histogram of porosity and permeability in Qingxi Sag. (a) Histogram of porosity distribution of the Xiagou Formation in Qingxi Sag. (b) Histogram of permeability distribution of the Xiagou Formation in Qingxi Sag.

studied reservoir, 1525 porosity and 584 permeability values from 15 wells, such as Liu9, Long104, and Qing2-4 wells, were calculated. As illustrated in Figure 3(a), reservoir porosity in the study area generally reaches less than 10%, mainly between 1% and 7%, and features poor reservoir characteristics. Figure 3(b) shows that reservoir permeability in the study area mainly lies between 0.1×10^{-3} and $2 \times 10^{-2} \mu\text{m}^2$; thus, the permeability of reservoirs is poor. Permeability values indicate that the Xiagou Formation reservoir in Qingxi Sag is strongly compacted and its permeability and porosity are low.

Based on the permeability-porosity relationship, Figure 4 shows that with increasing porosity, permeability generally increased, but no mutual control relationship was observed between them. For rock samples with the same porosity, the maximum difference in permeability values was nearly 4 times. For rock samples with the same permeability, maximum difference in porosity values approximated 5%. Thus, including pore-throat size, allocation, and connectivity, the complex pore structure of a tight reservoir more significantly influenced the pore and permeability of the reservoir.

4.1.2. Occurring Characteristics of Movable Fluid in Reservoir.

The distribution of a saturated movable fluid in the study area ranged from 11.42% to 45.52% and incurred an average of 26.73%, indicating the low concentration of the movable fluid in the studied reservoir and the strong heterogeneity of fluid occurrence. A strong positive correlation was found between permeability and movable fluid saturation, with the correlation coefficient reaching 0.7632 (Figure 5(a)). In comparison, the correlation of porosity with migrating fluid saturation significantly weakened, presenting almost no remarkable interaction (Figure 5(b)). The role of permeability in controlling movable fluid saturation is much more significant than that of porosity, whereas the development of secondary pores and microcracks and other factors exhibit strong control on reservoir permeability [52–54]. Our results indicate that movable fluid saturation is also affected by the growth of secondary pores and microcracks. Better permeability of a reservoir results in a stronger seepage ability of rocks and a smaller bound impact on the movable fluid, which develops in pores larger than the cutoff pore diameter, thus causing more significant saturation of the corresponding

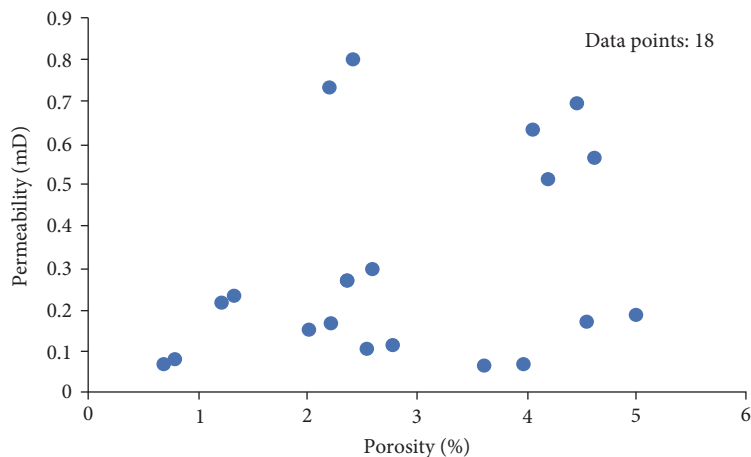
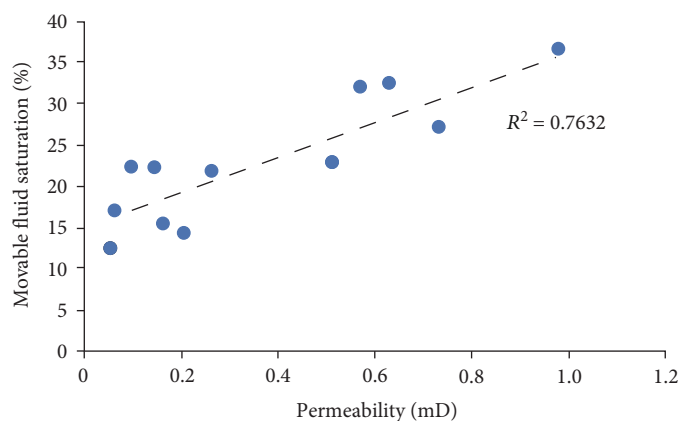
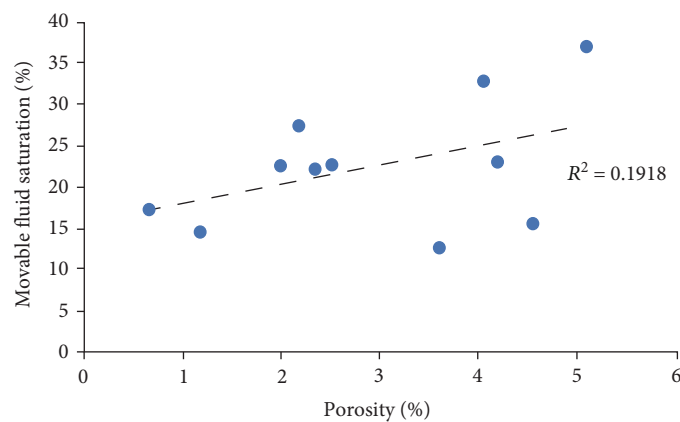


FIGURE 4: Correlation between rock porosity and permeability of the Xiagou Formation in Qingxi Sag.



(a)



(b)

FIGURE 5: Scatter plot of movable fluid saturation in Qingxi Sag. (a) Correlation between permeability and movable fluid saturation in the Xiagou Formation of Qingxi Sag. (b) Correlation between porosity and movable fluid saturation of the Xiagou Formation in Qingxi Sag.

movable fluid. However, the influence of porosity on the saturation of a movable fluid still presents uncertainty.

4.2. Size and Distribution of Pore-Throat. The average pore diameter, which reflects the average pore size of reservoir rocks, was distributed widely and ranged from 0.06 to 11.69 μm (mean = 2.39 μm ; Figure 6(a)). The reservoir

space is dominated by nanopores and micropores. Median radius ranged from 16.32 to 161.8 μm (mean = 89.08 μm ; Figure 6(b)). Median radius is the pore-throat radius representing 50% mercury saturation in the mercury intrusion experiment. A larger median radius indicates better pore-throat seepage performance. Therefore, pore-throats in the study area possess poor seepage capacity.

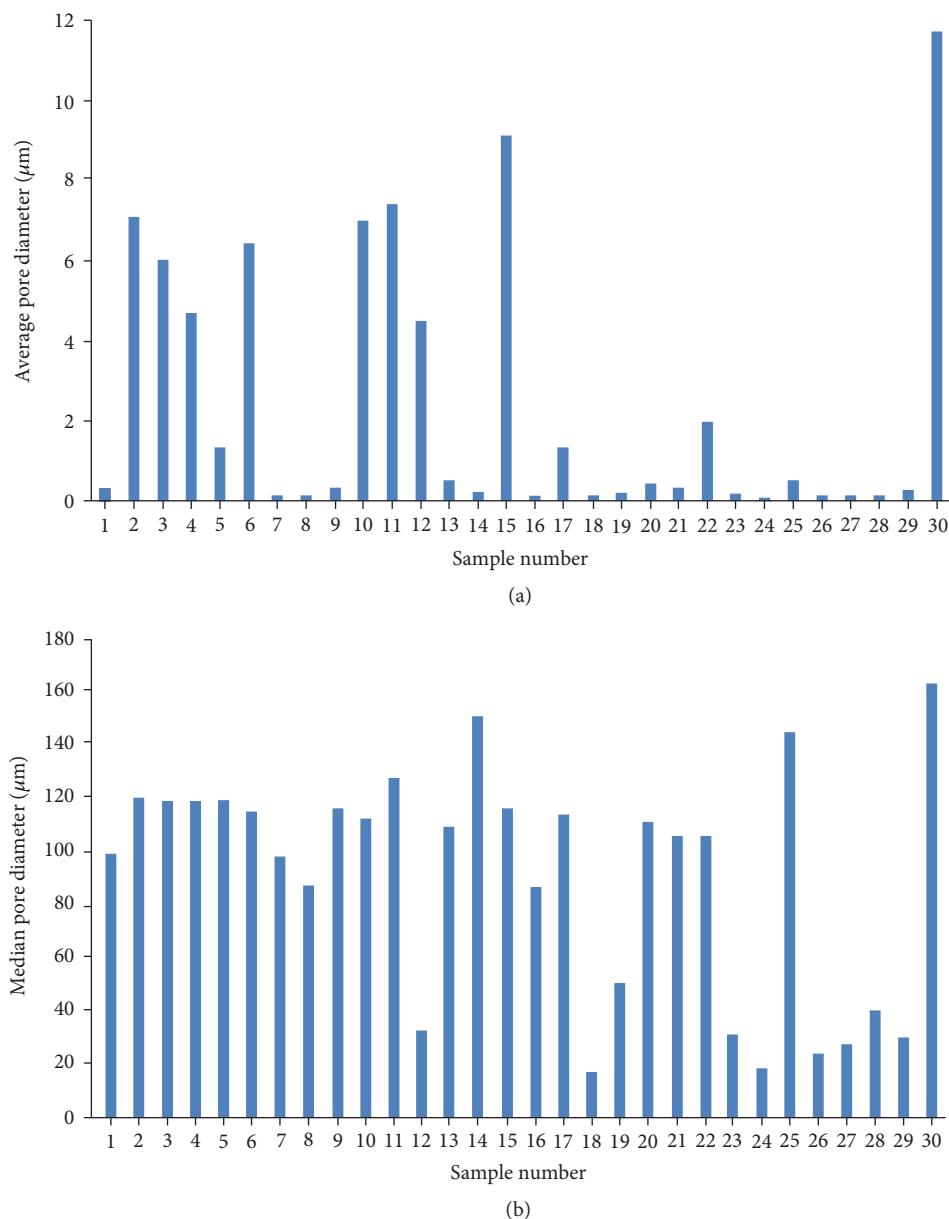


FIGURE 6: Histogram of pore size distribution in Qingxi Sag. (a) Distribution of average pore diameter of the Xiagou Formation in Qingxi Sag. (b) Median pore diameter distribution of the Xiagou Formation in Qingxi Sag.

As shown in the overlay of the T_2 spectral curve (Figure 7), rock pore diameter distribution in the study area is mainly unimodal, bimodal, or single- and double-peaked transition states with pore diameters generally concentrating at $10\ \mu\text{m}$. The content of unimodal and bimodal pore diameters mainly falls within $0.01\text{--}0.1$ and $1\text{--}10\ \mu\text{m}$. Pore diameters of single and double peaks in a transitional state were all concentrated at $10\ \mu\text{m}$ but were mostly within $0.01\text{--}0.1\ \mu\text{m}$. The reservoirs in the study area feature a complex pore structure, and the peak and ranges of pore diameters were significantly different among different samples.

Typical unimodal samples, such as Long104-26 samples, can be observed from Figure 8(a). Pore diameters are mainly concentrated within $0.01\text{--}0.07\ \mu\text{m}$, the content peak of pore diameters are approximately $0.03\ \mu\text{m}$, and the remaining

content of pore diameters is notably small. In the research area, rocks with unimodal pore diameter distribution were widely developed. Considering Long104-26 samples as representative, pore diameter distribution was mainly characterized by micropores, followed by mesopores, whereas macropore content was the lowest. The pore-throat type features small reservoir capacity and poor seepage capacity. Typical bimodal samples, such as the Q2-4-04 core, can be observed from Figure 8(b). Pore diameters were mainly concentrated between $0.01\text{--}0.22$ and $2\text{--}10\ \mu\text{m}$, with a peak pore diameter content of $0.04\ \mu\text{m}$. Extremely low content was observed between 0.22 and $2\ \mu\text{m}$. In this study area, rocks with bimodal pore diameter distribution were widely developed. Considering the Q2-4-04 core as representative, pore diameter distribution was mainly comprised of micropores

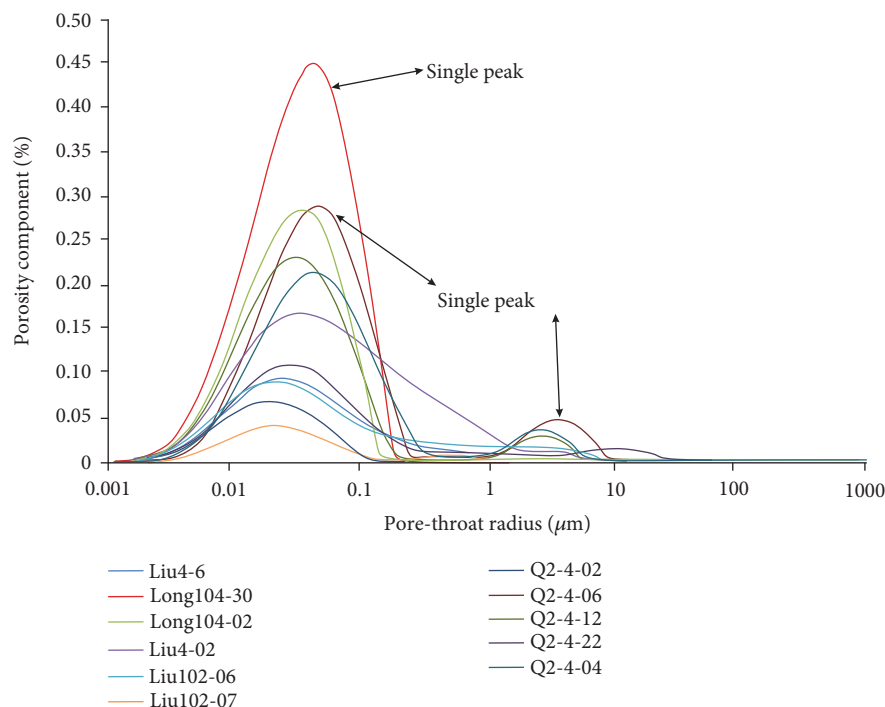


FIGURE 7: Core NMR characteristic curves of the Xiagou Formation in Qingxi Sag.

and macropores, whereas mesopore content was extremely low. Pore-throat type exhibited better reservoir capacity and poor seepage ability. Single- and double-peaked transition state samples, such as the Liu4-02 core, can be observed from Figure 8(c). Pore diameters were mainly concentrated in the range of 0.01–0.69 μm , the peak of pore diameter content was 0.02 μm , and a decrease was noted in the percentage of micropore content. Rocks with single-double peaks of transitional pore diameter distribution in the study area were rarely developed, as represented by Liu4-02. Pore diameter distribution was dominated by micropores and mesopores. This pore-throat type presents good reservoir capacity and strong seepage ability.

4.3. Reservoir Pore Types. The Xiagou Formation in Qingxi Sag possesses intergranular, dissolution, intragranular, inter-crystal, and organic pores.

(1) Intergranular pore implies primary porosity. Intergranular pores refer to the pores between particles, matrix, and cement, pores supported by particles or matrix, and intergranular residual pores with a reservoir property that is not fully filled with matrix and authigenic cement [55, 56]. The studied Xiagou Formation is in the late diagenetic stage. As a result of the effects of strong compaction and authigenic cementation, most of the intergranular pores feature smaller pore diameters. Well-preserved intergranular pores occur mostly between organics and brittle minerals and are supported and protected by brittle minerals [52, 53]. The intergranular pores in the study area showed good overall connectivity, significantly con-

tributing to the permeability of the reservoir. Such pores possess good oil and gas reservoir properties and good seepage ability and are mainly elliptical or irregular, and their diameters span from the nanometer level to the micrometer level (Figures 9(a) and 9(b)).

- (2) Dissolution pores occur at the edge of interstitial particles and distributed between particles [57]. Such pore types are mostly irregularly shaped, elongated, or honeycombed due to the remaining undissolved material [52, 53]. SEM showed that dissolution not only formed intergranularly dissolved pores, enlarged pores, and throat but also connected the original pores which were not connected to each other. Pore diameter is mostly at the micropore level, effectively improving the reservoir and its seepage capabilities (Figure 9(c)).
- (3) The intragranular pores consist of internal primary pores formed from particle deposition, and secondary pores resulting from diagenesis and later transformation [58]. Elliptical and irregular intragranular pores can be observed in the SEM images of the reservoir area. The sizes of pore diameter are mostly at the nanoscale, and most of them are associated with intergranular pores. At the same time, the intragranular pores were also distributed in the easily dissolved minerals, such as dolomites, in the study area. Most intragranular pores were isolated pores, which cannot be well connected with the surrounding pore-throat. Thus, intragranular pores exerted minimal impact on pore and permeability of the reservoir (Figure 9(d)).

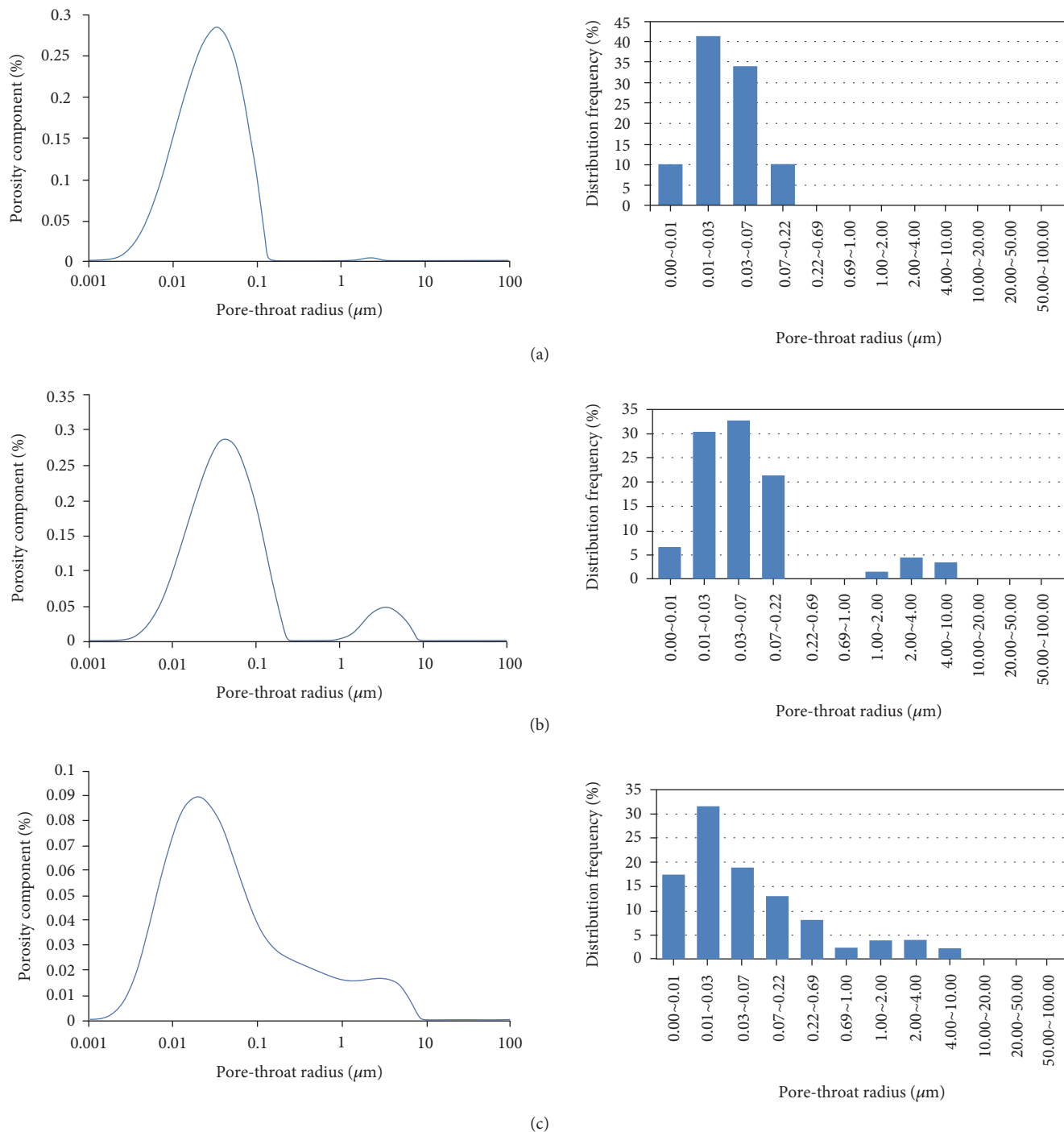


FIGURE 8: Distribution of pore throat radius in Qingxi Sag. (a) Long104-26 pore diameter of the Xiagou Formation in Qingxi Sag. (b) Pore diameter distribution of Q2-4-06 at the Xiagou Formation in Qingxi Sag. (c) Pore diameter distribution of Liu4-02 at the Xiagou Formation in Qingxi Sag.

(4) Intercrystal pores correspond to the pores between carbonate mineral crystals, which are formed by recrystallization and dolomitization [59, 60]. In the study area, the intercrystal pores between carbonate rock and clay slime crystal were developed. Results showed the micropore diameters, which were mostly at the nanoscale and were mainly

observed in argillaceous dolomite. Intercrystal pores are the basic pores in dolomite and feature micropore diameter. However, these pores are abundant in dolomite and can dissolve and spread into dissolved intercrystal pores, which are also critical in oil and gas reservoirs and percolation (Figures 9(e) and 9(f)).

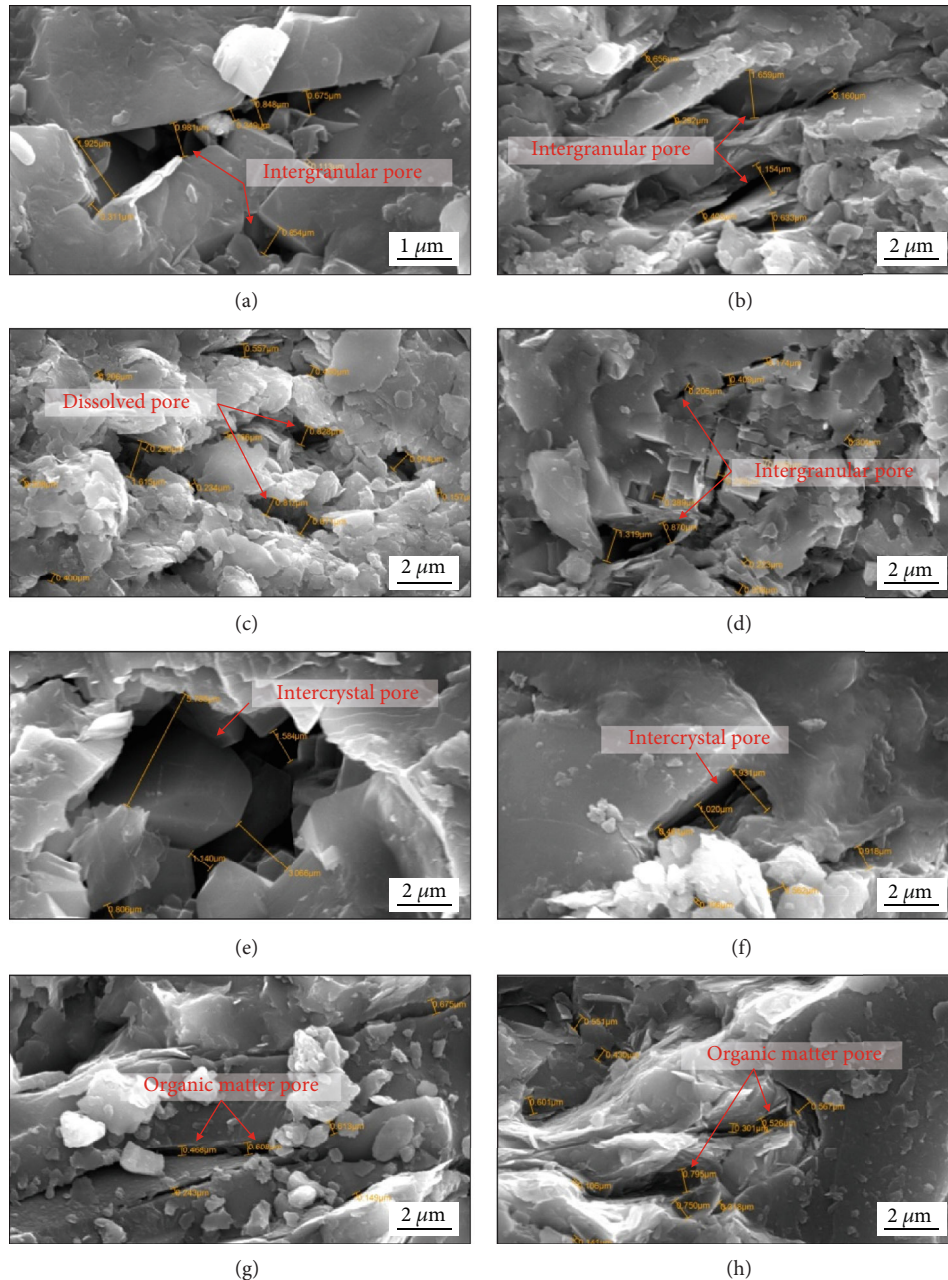


FIGURE 9: Scanning electron micrographs of the Xiagou Formation reservoir in Qingxi Sag. (a) Liu4-02, 4486.6 m, gray-black dolomitic mudstone, intergranular pores. (b) Long104-26, 4343.3 m, gray dolomitic mudstone, intergranular pores. (c) Q2-4-08, 3884.3 m, gray silt-bearing dolomitic mudstone, dissolved pores. (d) Q2-4-04, 3879.83 m, dark gray silt-bearing dolomitic mudstone, intragranular pores. (e) Q2-4-50, 4307.77 m, gray dolomitic siltstone, intercrystal pores. (f) Long104-26, 4343.3 m, gray-black dolomitic mudstone, intercrystal pores. (g) Long104-26, 4343.3 m, gray-black dolomitic-like mudstone, organic matter pores. (h) Q2-4-08, 3884.33 m, gray silty sand dolomitic mudstone, organic matter pores.

(5) Organic matter pores form during the transition from organic matter to hydrocarbons; such a process will generate residual pores [61]. Organic pore diameter reaches the nanoscale level. In the study area, strip-shaped organic matter was developed in the reservoir, and organic matter pores were partially developed in a small amount of organic matter. The study shows that increased maturity of organic matter will generate more reserved pores after hydrocarbon for-

mation. From the laboratory test, the studied Xiagou Formation was mainly at 0.7% to 1.3% maturity, which has no specific benefit to the development of organic matter pores. Most organic matter pores were isolated pores, and their pore diameters were notably smaller than those of intergranular and intragranular pores. Organic matter pores also feature poor pore connectivity, contributing little to the permeability of the reservoir (Figures 9(g) and 9(h)).

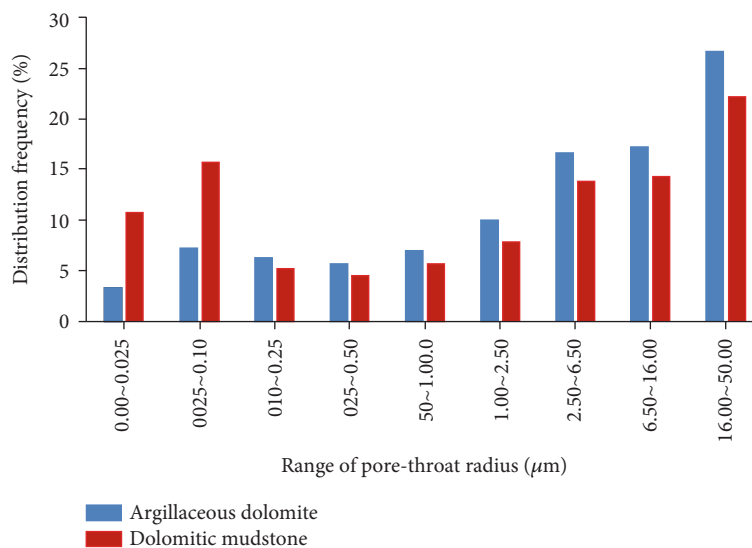


FIGURE 10: Distribution of pore-throat radius of the Xiagou Formation in Qingxi Sag.

5. Discussion

5.1. Influence of Reservoir Pore-Throat Size on Physical Properties. Considering 0.1 and $1\ \mu\text{m}$ as boundaries, the studied pores were separated into macropores, mesopores, and micropores. The pores with sizes larger than $1\ \mu\text{m}$ represented macropores, the pores with sizes ranging from $0.1\ \mu\text{m}$ to $1\ \mu\text{m}$ represented mesopores, and the pores with sizes smaller than $0.1\ \mu\text{m}$ represented micropores. By counting the average pore diameter distribution of argillaceous dolomite and dolomitic mudstone (Figure 10), pore content of each interval of dolomitic mudstone showed two ends, whereas micropores and macropores yielded higher contents than mesopores. The pore content of argillaceous dolomite in each distribution range increased with pore diameter and was dominated by macropores. Argillaceous dolomite features a reservoir space dominated by macropores and thus possesses better properties than dolomitic mudstone, which mainly consists of micropores and macropores.

To clarify the influence of pore-throat size on average pore diameter, the correlations between macropores, mesopores, and micropores with average pore diameters were analyzed. The comparative analysis in Figure 11 shows the strong correlation between average pore diameter and macropores (correlation coefficient: 0.5725) and micropores (correlation coefficient: 0.5867). However, a weak correlation was observed between mesopores and average pore diameter, with a correlation coefficient of 0.242. When macropore content increased, average pore diameter increased. When the content of micropores increased, average pore diameter decreased. Variations in mesopore content showed no remarkable regularity on average pore diameter. The contents of micropores and macropores exhibited a strong controlling effect on average pore diameter inside the reservoir. This result is due to the micropores and macropores dominating the reservoir area; mesopore content is controlled by macropore and micropore contents. The reservoir

spaces in the study area are dominated by micropores and macropores, and their contents control reservoir capacity.

As shown in Figure 12, with a correlation coefficient of 0.9369, average pore diameter featured a strong correlation with permeability, indicating that average pore diameter directly determines reservoir seepage capacity. At the same time, changes in the content of micropores and macropores significantly affect average pore diameter. Therefore, studies should analyze the correlation between permeability and micropores, mesopores, and macropores.

In Figure 13, we can observe the very strong correlation between the content of macropores and micropores with permeability, with correlation coefficients of 0.5851 and 0.5886, respectively. However, a weak correlation was noted between mesopore content and permeability, with a correlation coefficient of 0.2712. With increasing macropore content, permeability notably increased until the content reached more than 85%. The explanation for this observation is as follows. When macropore content accounted for a sufficient proportion of pore diameter, the connectivity of pore-throats will naturally improve and permeability will increase (Figure 13(a)). When the content of micropores measured less than 3%, the permeability of the reservoir notably increased because the micropores represent the throat size of the reservoir. When the content of micropores is low, the content of a small throat naturally declines, and its binding effect on pores also weakens, whereas reservoir permeability increases (Figure 13(c)). When mesopore content totaled less than 7%, reservoir permeability was divided into two types: the first type indicates that permeability increased notably, whereas the other indicates no change. This result was attributed to the fixed mesopore content, whereas the contents of micropores and macropores determine permeability (Figure 13(b)). Therefore, the configuration relationship between macropores and micropores in the reservoir decides the physical properties in the study area. When macropore content reaches higher than 85%, or when micropore content measures lower than 3%, the permeability of the reservoir improves.

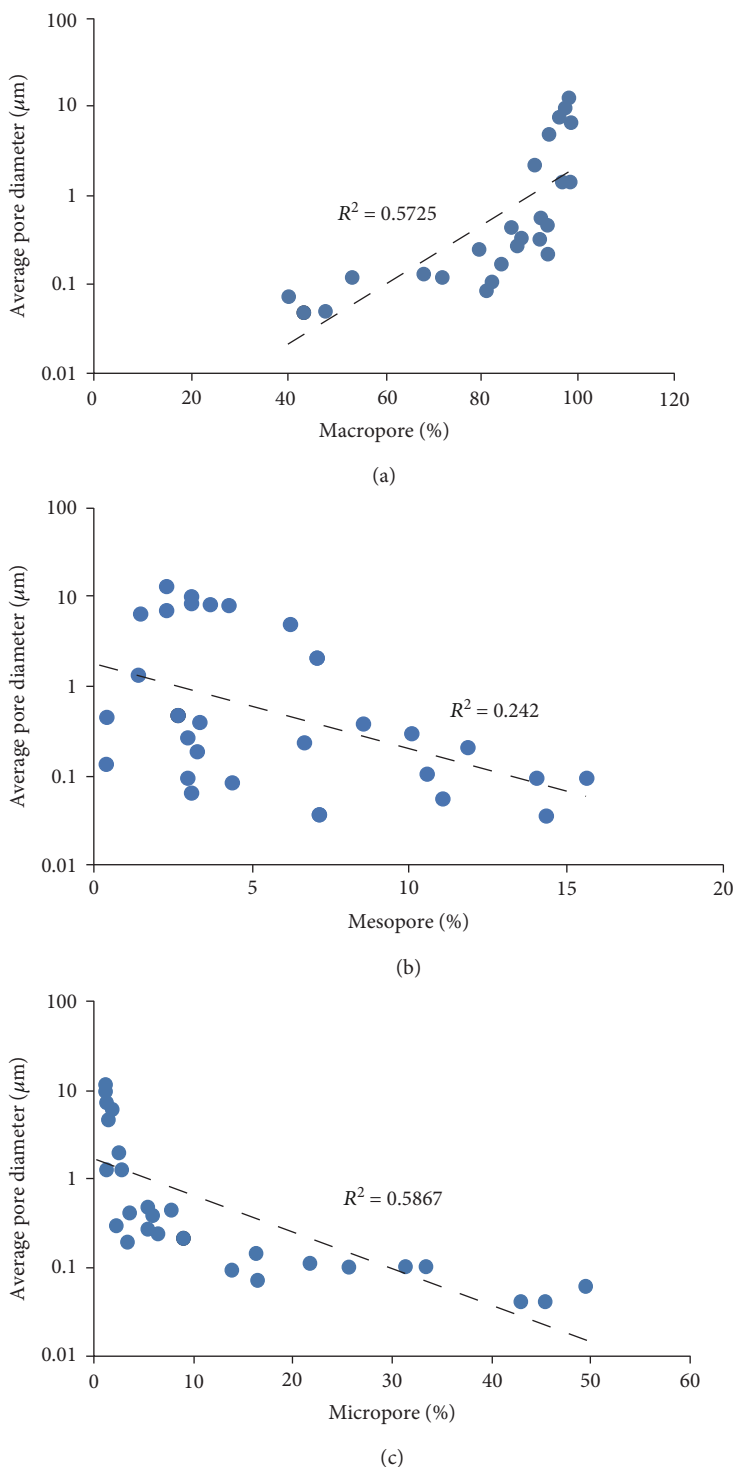


FIGURE 11: Relationship between different pore sizes and average pore size in Qingxi Sag. (a) Relationship between average pore diameter and macropore content of the Xiagou Formation in Qingxi Sag. (b) Relationship between average pore diameter and mesopore content in the Xiagou Formation of Qingxi Sag. (c) Relationship between average pore diameter and micropore content of the Xiagou Formation in Qingxi Sag.

5.2. Impact of Pore-Throat Distribution Characteristics on Reservoir Physical Properties. The pore-throat sorting coefficient of the samples from the Xiagou Formation in the study area ranged from 1.39 to 3.12, indicating a medium-to-poor sorting. The correlation between movable fluid saturation

and sorting coefficient was strong, with a coefficient of 0.753 (Figure 14(a)). The sorting coefficient and movable fluid saturation are exponential. With increasing sorting coefficient, mobile fluid saturation will increase. However, when sorting coefficient continually increases to some

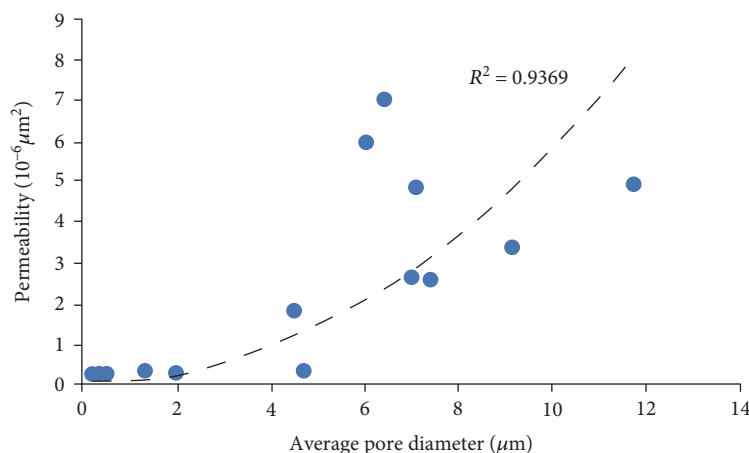


FIGURE 12: Relationship between average pore diameter and permeability of the Xiagou Formation in Qingxi Sag.

extent, movable fluid saturation will decrease. This result is attributed to the pore sizes, which are dominated by micropores and nanopores, in the tight reservoir of the study area. At a very low pore-throat sorting coefficient, the small throats will account for most of the throats and exert no or little effect on seepage. Thus, this explains why the movable fluid saturation is very small at this time. With increasing sorting coefficient, the extent of pore-throat distribution was wider, and the percent of macroporous throat and saturation of movable fluid increased. When the sorting coefficient is extremely high, pore-throat heterogeneity will be enhanced, pore structure will be more complex, and saturation of the movable fluid will be naturally decreased [62]. Therefore, when the sorting coefficient is very low or high, the value of movable fluid saturation will show no considerable enlargement when sorting coefficient reaches between 1.8 and 2.5, that is, at a wide distribution of pore-throats and a high ratio of mesopore to macropore content of reservoir rock, saturation of movable fluid will reach the highest, and a high content of movable fluid in the reservoir will be observed.

As depicted in Figure 14(b), the correlation coefficient between sorting coefficient and permeability has reached 0.5582, indicating a strong correlation. The sorting coefficient and porosity are exponential. The change regulation between permeability and sorting coefficient is similar to that between movable fluid saturation and the sorting coefficient. With an increasing sorting coefficient, the permeability of the reservoir will increase and then decrease. The sorting coefficient reflects the distribution regulation of pore-throats in the reservoir. At a low sorting coefficient, pore-throat sorting will be moderate, and the pore-throat will be small. Thus, reservoir permeability will naturally be low. When the sorting coefficient increases, pore-throat distribution will widen, and mesopore and macropore contents, permeability of the reservoir, and permeability will increase. When sorting difference is poor, micropores, mesopores, and macropores are all distributed, but mesopores and macropores are bound by tiny throats where the fluid cannot flow freely, and reservoir permeability decreases. Porosity characterizes the reservoir capac-

ity of reservoir rocks, which are naturally not significantly related to the distribution characteristics of pore-throats.

Skewness is the symmetry parameter of pore-throat frequency distribution, which reflects the relative position of modes, and is called coarse skewness when the mode is in the coarse-pore end and fine skewness when the mode is in the fine-pore end; improved coarse skewness was observed for the studied reservoir [63–65]. The movable fluid saturation and skewness are strongly correlated, with a coefficient of 0.6212 (Figure 15(a)). This result is explained as follows: when skewness increases, the proportion of macropores in the pores becomes larger than that of the micropores. Thus, the saturation of the movable fluid also increases. Correlation was observed between skewness and permeability, with a correlation coefficient of 0.4938 (Figure 15(b)). With an increasing skewness value, macropore content increased, favoring seepage of the reservoir. No notable correlation was detected between skewness and porosity because the type of the studied reservoir space is dominated by macropores or mesopores and micropores, which cannot affect the size of the total reservoir space. Compared with the sorting coefficient, skewness exerts a weak influence on effective porosity of the movable fluid. The controlling effect of pore-throat allocation on effective porosity is reflected in the uniformity of pore-throats, but it does not mean that the bigger the pore size, the better. Thus, the configuration relationship of pore-throats plays an important role.

5.3. Influence of Reservoir Pore-Throat Connectivity Characteristics on Reservoir Physical Properties. Movable fluid saturation and permeability are strongly correlated with mercury removal efficiency at coefficients of 0.7068 and 0.7869, respectively (Figure 16). When mercury removal efficiency increased, saturation of the movable fluid and permeability increased. During mercury removal, the finer throats first emptied the mercury, destroying the connectivity of the entire pore space; as a result, a portion of the pores and throats became separated, and no mercury was emitted any more, reflecting the favorable regulating effect of a small throat on the pore fluid [52, 63]. When rock mercury

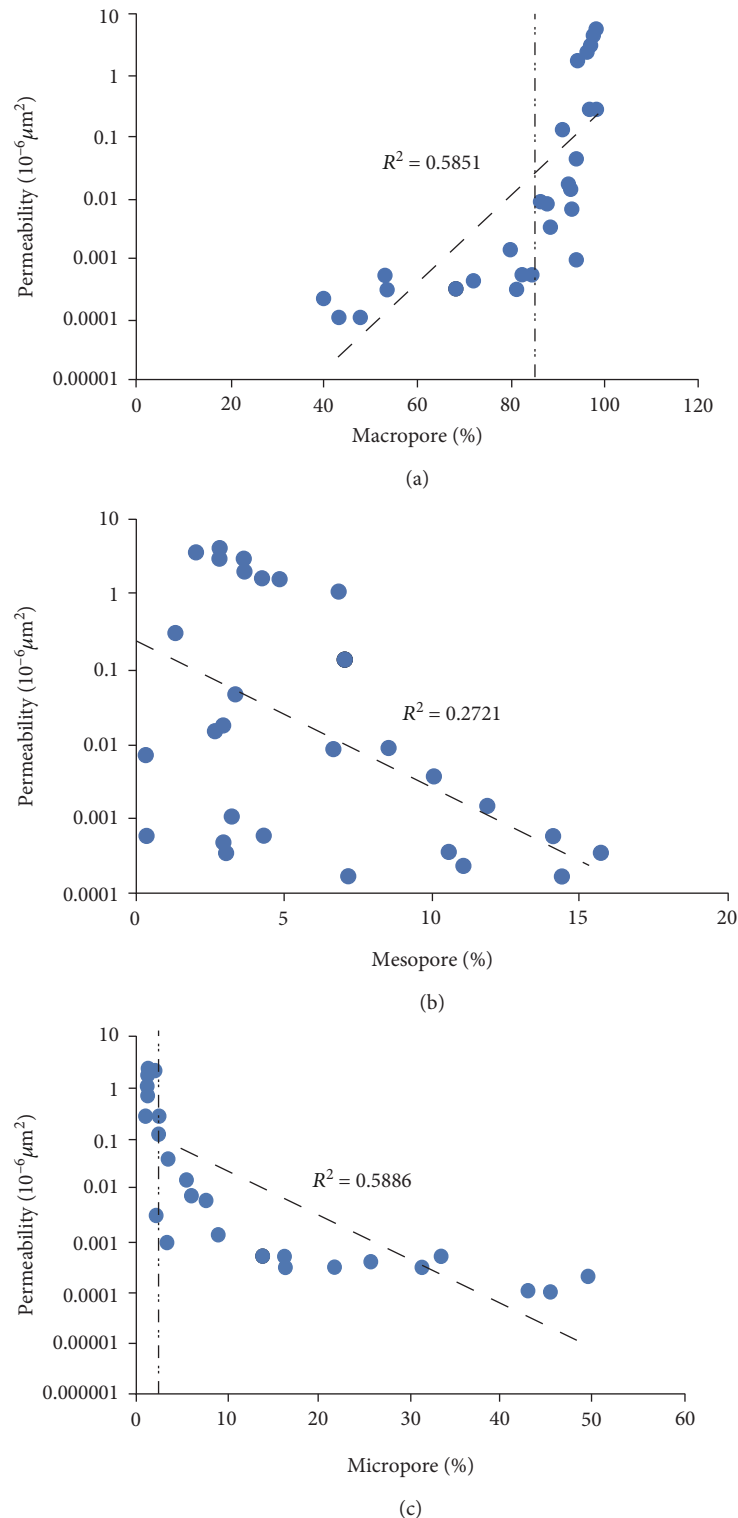


FIGURE 13: Relationship between pores of different scales and average pore size in Qingxi Sag. (a) Relationship between permeability and macropore content of the Xiagou Formation in Qingxi Sag. (b) Relationship between permeability and mesopore content of the Xiagou Formation in Qingxi Sag. (c) Relationship between permeability and micropore content of the Xiagou Formation in Qingxi Sag.

removal efficiency was low, the development of fine pore-throats in the rock was relatively high, and the saturation of the movable fluid and the permeability in the reservoir were naturally low. When mercury removal efficiency increases,

the proportion of macropore-throats and mesopore-throats, movable fluid saturation, and permeability will increase. Mercury removal efficiency exhibited good correlation with movable fluid saturation and permeability, which can

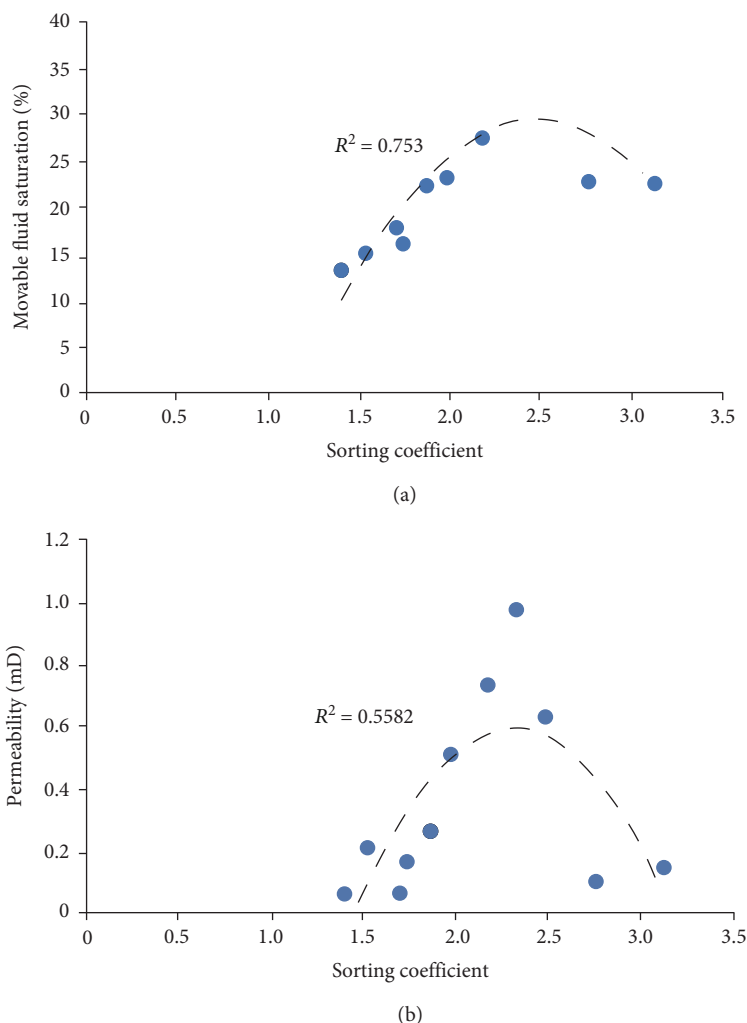


FIGURE 14: Relationship between movable fluid saturation, permeability, and separation coefficient in Qingxi Sag. (a) Diagram of the relationship between sorting coefficient and movable fluid saturation in the Xiagou Formation, Qingxi Sag. (b) Relation diagram between sorting coefficient and permeability of the Xiagou Formation in Qingxi Sag.

indirectly uncover the size of mobile fluid saturation and permeability in the reservoir. Notably, when micropores and macropores were mainly developed in the reservoir, low mercury removal efficiency was observed from the reservoir, but saturation of the movable fluid in the reservoir was high because the micropores impeded mercury removal, and at the same time, macropores enlarged the saturation of mobile fluid. Therefore, the level of connectivity is crucial in the physical properties of the reservoir.

5.4. Characteristics of Reservoir Pore-Throat Network System. Porosities of the Liu4-06 and Long102-06 samples reached 2.47% and 2.21%, respectively, with permeabilities of 0.143 and 0.059 mD. The two samples presented similar porosity, but the difference in permeability was nearly 3 times. To confirm the differences in pore-throat connectivity between the two samples, a 3D nano-CT imaging method was performed.

Throat-pore ratio is defined as the ratio of the rock throat radius to its connected pore radius. A larger throat-pore ratio indicates a larger throat radius, a smaller pore

radius, a closer connection of pore and throat radius, and a stronger rock seepage ability. Figure 17(a) shows the histogram of the throat-pore ratio for the two samples, Liu4-06 and Long102-06, in which the Liu4-06 sample featured three throat ratio intervals between 0 and 0.2, 0.2 and 0.4, and 0.4 and 0.6 and a percentage content smaller than that of the Long102-06 sample. The percentage of sample No. 4-06-06 was higher than that of the Long102-06 samples in the throat-pore ratio range of 0.6 to 0.8 and 0.8 to 1.0, whereas the percentage content of the Liu4-06 sample was significantly higher than that of the Long102-06 sample. The throat radius of the Liu4-06 sample is much closer to the size of the connected pore radius than that of the Long102-06 sample; the pore-throat also showed good connectivity.

This paper next compared and analyzed the distribution of the finest sectional area of the throat of the Liu4-06 and Long102-06 samples. Figure 17(b) shows that the content of the finest sectional area of the throat of the Liu4-06 sample was notably higher than that of the Long102-06 sample in two intervals over $80 \mu\text{m}^2$, and the content in four intervals

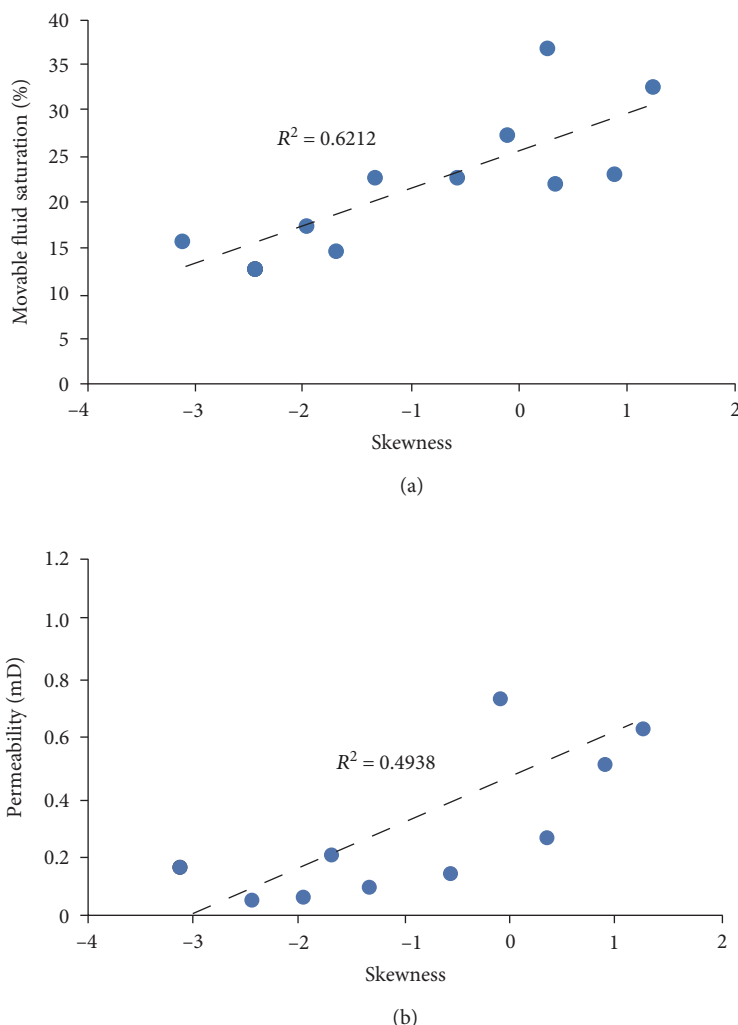


FIGURE 15: Relationship between movable fluid saturation, permeability, and skewness in Qingxi Sag. (a) Relationship between skewness and movable fluid saturation of the Xiagou Formation in Qingxi Sag. (b) Relationship between skewness and permeability of the Xiagou Formation in Qingxi Sag.

of less than $80 \mu\text{m}^2$ was generally lower than that of the Long102-06 sample. This result indicates that compared with the Long102-06 sample, the proportion of the large throat content in the Liu4-06 sample is higher, thus favoring fluid flow in the rock pore and indicating good pore-throat connectivity.

As observed from the 3D pore-throat connectivity diagram of the two samples, Liu4-06 and Long102-06 (Figure 18), the same color in the local area represents the interconnected pore-throats connected with each other. In the local pore-throat interconnection area of the Liu4-06 sample, volume is visibly higher than that of the Long102-06 sample and is widely distributed in the reservoir. Thus, Liu4-06 features higher permeability than that of the Long102-06 sample.

In summary, a large throat-pore ratio with a large sectional area at the finest part of the throat and with good local pore-throat connectivity and pore-throat connection area is widely distributed in the reservoir. The pore-throats will exhibit good connectivity and high permeability which is

caused by the higher volume of the local pore-throat interconnection area and wider distribution in the reservoir. This observation primarily explains the similar porosities of samples Liu4-06 and Long102-06 but the remarkably higher permeability of Liu4-06.

5.5. Classification of Reservoir Pore Structure. Based on permeability, movable fluid saturation, sorting coefficient, and mercury removal efficiency, pore structures were classified into three types (Table 1). The influencing factors of the physical properties of various pore structures were analyzed from a diagenetic perspective.

5.5.1. Type I. This pore structure is good and is a small-pore-thin-throat type. Movable fluid saturation exceeds 20%, mercury removing efficiency is 20%-30%, permeability is above 0.1 mD, and sorting coefficient is higher than 1.5 (Table 1). Maximum mercury saturation of this pore structure neared 70%, displacement pressure was small, and mercury injection curves follow a more remarkable platform, indicating the

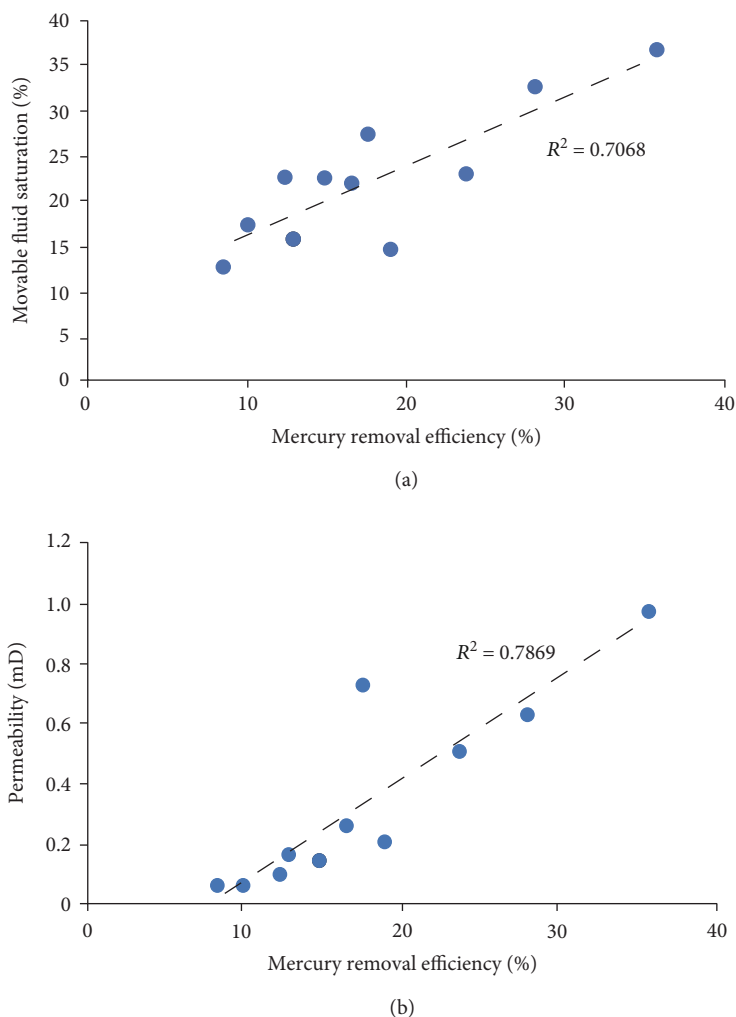


FIGURE 16: Relationship between movable fluid saturation, permeability, and mercury removal efficiency in Qingxi Sag. (a) Relation diagram of mercury removal efficiency and movable fluid saturation in the Xiangou Formation of Qingxi Sag. (b) Relationship between mercury removal efficiency and permeability in the Xiangou Formation, Qingxi Sag.

more concentrated effective throat distribution of rocks and good configuration relationship of the pore-throat. The T_2 curve shows single- and double-peak transition states, indicating that this type of pore structure contains a certain number of macropores (Figure 19).

A few clay minerals exist in this type of pore structure. Most pore types include intergranular and dissolved pores. The pore types are mainly controlled by lithology and diagenesis, while organic matter types and abundance contribute little to the pore types. The contact type is point or linear. Given the large amount of mudstone developed in the bottom section of the Xiangou Formation reservoir, a certain amount of organic acid will be produced simultaneously in mature hydrocarbon generation of organic matter. These acidic components will preferentially enter the reservoir adjacent to the mudstone, resulting in the dissolution of unstable components; this phenomenon is conducive to reservoir rock dissolution. Therefore, the type of pore structure is strongly affected by dissolution. Under the background of the strong compaction of the Xiangou Formation reservoir, dissolution is pivotal in strengthening the connectivity and

permeability of pore space. As observed in microscopic observation, feldspar and other minerals dissolved to form intragranular pores, and dissolution occurred along the cleavage and was followed by a honeycomb-like pattern. The intergranularly dissolved pores, which were formed by the dissolution of unstable components between particles, can be observed from the field of view with a pore diameter of 10–200 μm and with almost no particle filling the pores. The microfracture is well developed and features a mainly diagenetic fracture as the mineral components of sediments in the study area will undergo a series of changes given that self-burying and compaction and recrystallization will cause rock particles, which are conducive to microfracture formation, to expand and contract. The microfractures that developed along the grain boundaries can interconnect previously unconnected pores and significantly enhance the seepage capacity of the reservoir, whereas the large number of developed microfractures also act as an effective reservoir space (Figures 20(a) and 20(b)). Therefore, the type I pore structure features a large reservoir capacity and a strong seepage ability.

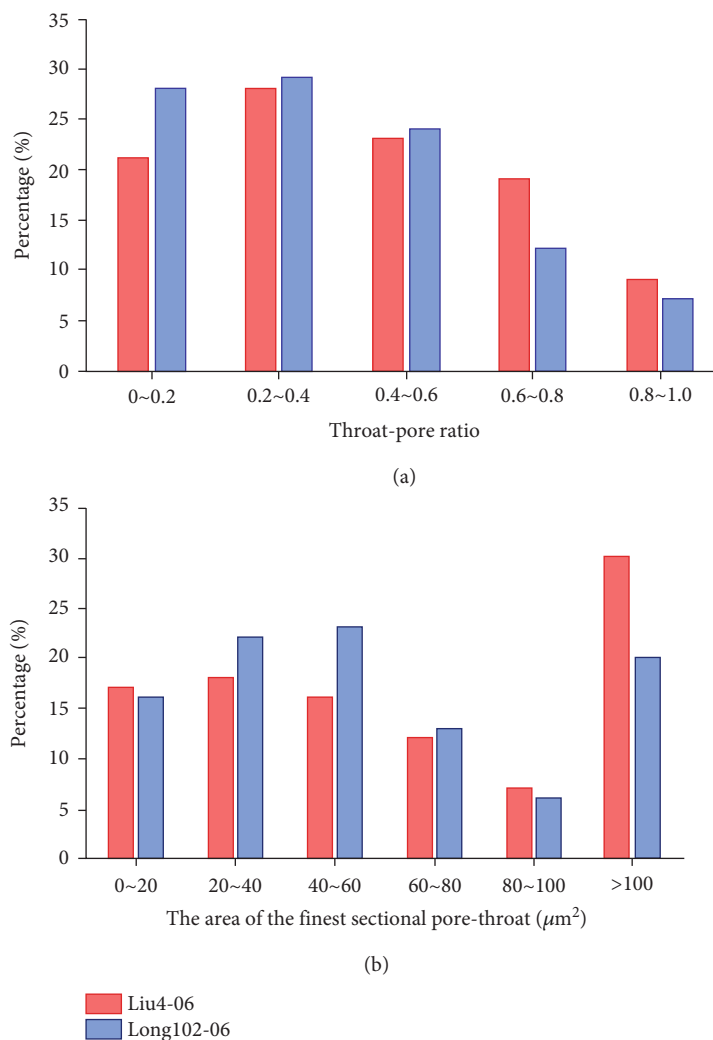


FIGURE 17: Relationship between pore-throat characteristics in Qingxi Sag. (a) Throat-pore ratio distribution in the Xiagou Formation, Qingxi Sag. (b) Distribution diagram of the finest sectional area of a pore-throat in the Xiagou Formation, Qingxi Sag.

5.5.2. *Type II*. This thin-pore–thin-throat type features a medium-to-poor structure. Its features include a movable fluid saturation of 10%-20%, a mercury removal efficiency of 10%-20%, a permeability basically of 0.05-0.1 mD, and a sorting coefficient of 1.0-1.5 (Table 1). The displacement pressure of this type of pore structure is notably higher than that of type I. The slope of the mercury injection curve increased and notably shifted to the right and upward, and the range of the effective radius of the throat was reduced. Maximum mercury saturation decreased to about 60%. The T_2 spectral curve is bimodal. The macropore content of this pore structure decreased, the micropore content increased gradually, and the pore-throat configuration is more complicated than that of type I (Figure 19).

Type II mainly develops intergranular and intercrystal pores. Mineral filling of pores is enhanced, and mineral coatings develop on the surface of particles, enhancing the viscous force of the pore-throat surface to the fluid and narrowing the throat. The pores also exhibit poor connectivity. Owing to the presence of acidic medium, such as hydrocarbons, the local environment was acidic, and cementation

became more developed, thus remarkably reducing pore space. Microfractures developed in small amounts with weak dissolution, intercrystal pores were mostly isolated, and the fluid inside the pores cannot participate in the flow and contributed little to reservoir seepage (Figures 20(c) and 20(d)). Therefore, the type II pore structure possesses better reservoir capacity and poor seepage.

5.5.3. *Type III*. This very poor pore structure is a micropore–microthroat type. Movable fluid saturation is below 10%, mercury removal efficiency is 5%-10%, permeability is below 0.05 mD, and sorting coefficient is lower than 1.0 (Table 1). The displacing pressure of this type is significantly large, indicating that the maximum pore-throat radius is significantly less than the first two types. The slope of the mercury injection curve is also very large and visibly offsets to the upper right. The pore-throat effective radius distribution range was dispersed, and maximum mercury saturation reached less than 60%. NMR T_2 spectrum distribution showed a unimodal curve, indicating the very low macropore content and very high micropore content (Figure 19).

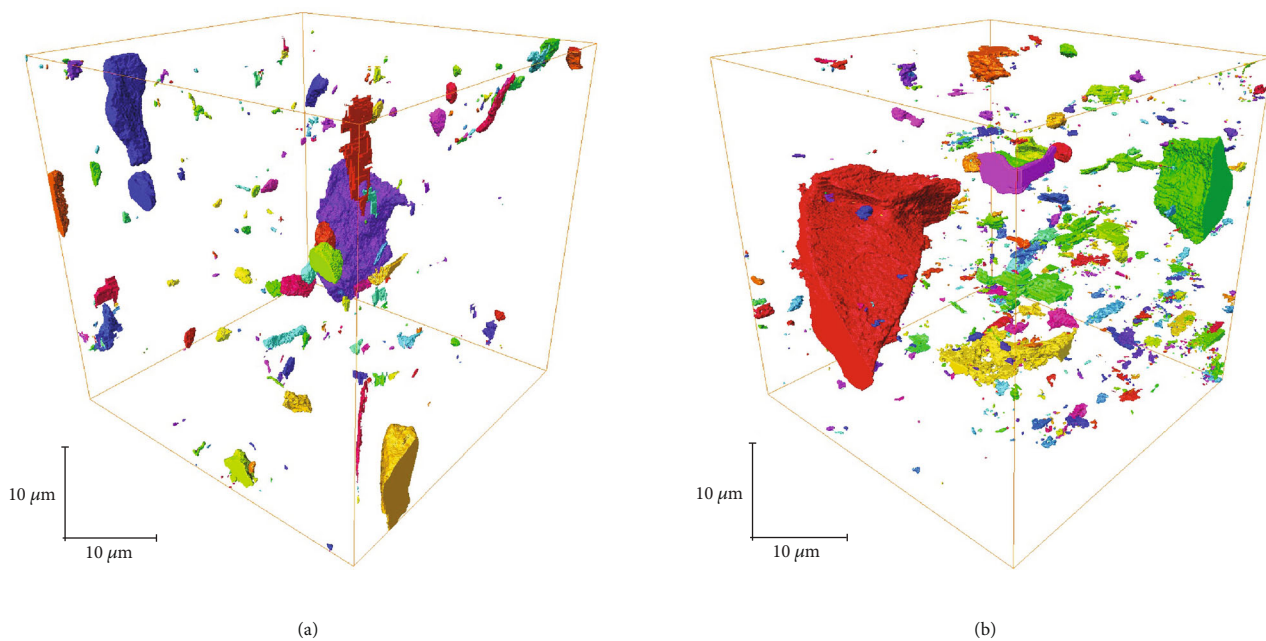


FIGURE 18: 3D pore-throat connectivity diagram of the Xiagou Formation core in Qingxi Sag. (a) 3D pore-throat connectivity diagram of Long102-06. (b) 3D pore-throat connectivity diagram of Liu4-06.

TABLE 1: Classification standard of pore structure of tight oil sandstone reservoir in Qingxi Sag of Jiuquan Basin.

Pore structure type	Movable fluid saturation (%)	Permeability (mD)	Mercury removal efficiency (%)	Sorting coefficient
I	>20	>0.1	20.0–30.0	>1.5
II	10–20	0.05–0.1	10.0–20.0	1.0–1.5
III	<10	<0.05	<10	<1.0

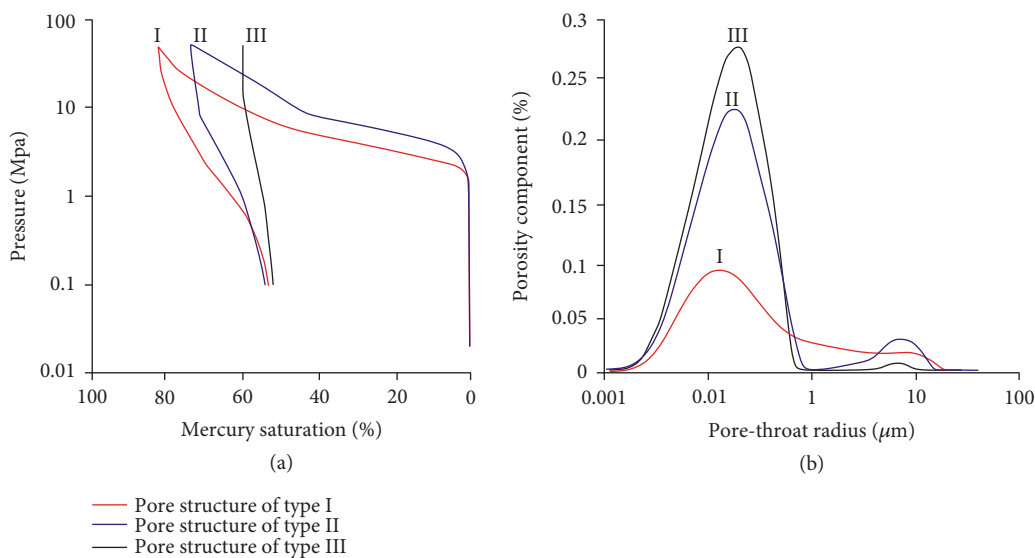


FIGURE 19: Relationship between mercury injection and nuclear magnetic resonance characteristics of three types of pore structures in the Xiagou Formation, Qingxi Sag. (a) Relationship between mercury saturation and pressure in different pore structures. (b) Relationship between pore-throat radius and porosity components in different pore structures.

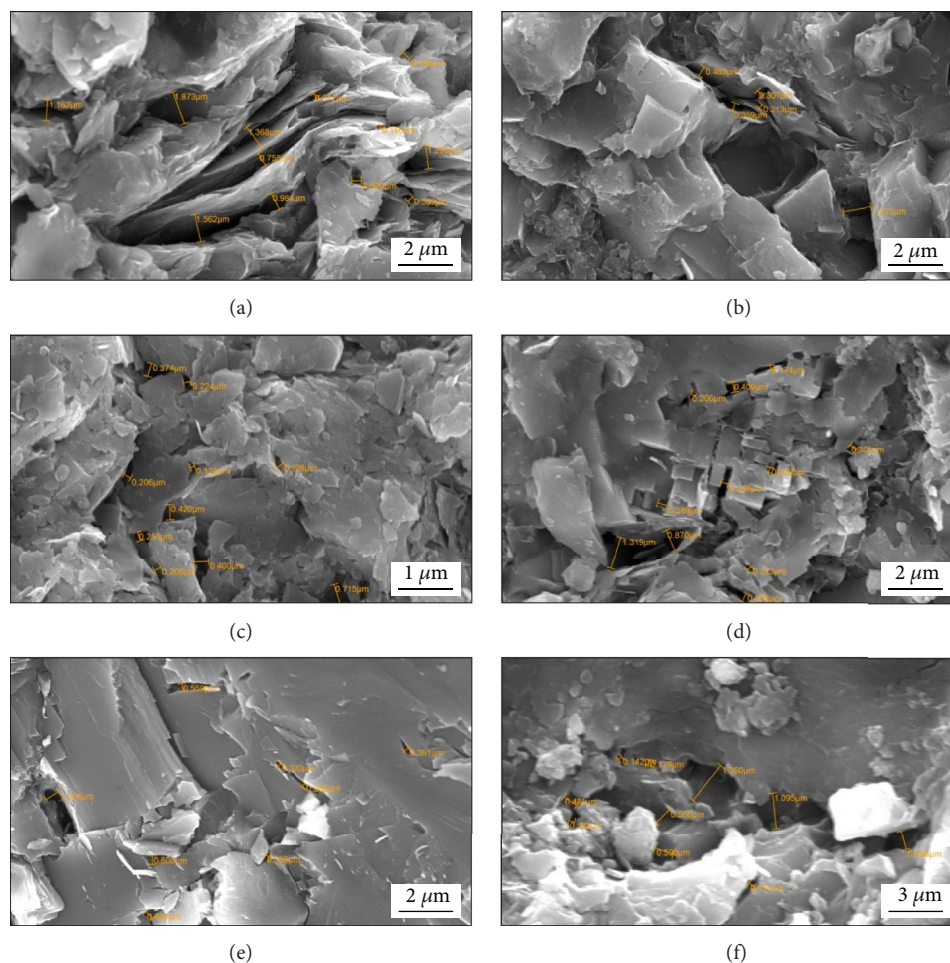


FIGURE 20: SEM characteristics of three types of pore structures in the Xiagou Formation, Qingxi Sag. (a) Q2-4-08, 3884.3 m, gray silt-bearing dolomitic. (b) Q2-4-10, 3903.5 m, gray argillaceous dolomite. (c) Q2-4-08, 3884.3 m, gray silt-bearing dolomitic mudstone. (d) Q2-4-04, 3879.83 m, dark gray silt-bearing dolomitic mudstone. (e) Long102-7, 4117.2 m, gray-black dolomitic mudstone. (f) Liu4-06, 4444.3 m, gray-black argillaceous dolomite, dotted throat.

This type contains undeveloped microfractures and is dominated by clay pores and micropores. Given the development of fine and silty sandstone with a high content of matrix in the Xiagou Formation reservoir in the study area, the fine grain size of sediments and buried depth in the geologic historical period resulted in compaction and densification of the reservoir, whereas the tight contact of particles worsened sorting. Clay minerals filled the pores and throats and not only divided intergranular pores into abundant binding pores, resulting in a narrower reservoir space, but also filled the throat into a bundle-like type, binding the flow of fluid in the pores and reducing seepage performance and also causing difficult dissolution (Figures 20(e) and 20(f)). Therefore, the type III pore structure features poor reservoir capacity and poor seepage ability.

6. Conclusions

- (1) The dolomitic mudstones and argillaceous dolomites of the Xiagou Formation reservoir in Qingxi Sag are

the main reservoirs of tight oil. Porosity is generally less than 10% and mainly ranges from 1% to 7%. Permeability mainly lies between 0.1×10^{-3} and $2 \times 10^{-3} \mu\text{m}^2$. Compaction transformation action is strong, and porosity, permeability, and storage capacity are low. Strong heterogeneity of tight reservoirs and a complicated pore-throat configuration relationship are the main reasons leading to low storage capacity and permeability

- (2) Intergranular, dissolution, intragranular, intercrystal, and organic matter pores were detected in the Xiagou Formation reservoir in Qingxi Sag. Among these pores, the intergranular and dissolution pores provide the main reservoir space. However, the intragranular and organic matter pores are mostly independent, which hardly contributed to the pore rate or permeation of the reservoir. Throats consist mainly of tube-shaped throats and sheet throats, and slightly of necking throats, dotted throats, and bend sheet throats, which are inconducive to fluid flow in the pores

- (3) In the studied formation, the average pore diameter of the reservoir totals $2.39\ \mu\text{m}$. Storage space is dominated by nanopores and micropores. Argillaceous dolomite is dominated by macropores, whereas dolomitic mudstone is dominated by micropores and macropores. Rock pore-throats are distributed either unimodally, which is mainly composed by micropores, or bimodally, which is dominated by micropores and supplemented by macropores. The configuration relationship between the contents of macropores and micropores bears importance and exerts a strong control on reservoir permeability. Overall, large throat-pore ratio, large finest sectional area of the throat, good connectivity of the local pore-throat, and pore-throat connectivity in the region are distributed among a wide range of rocks. Stronger connectivity of the pore-throat indicates higher permeability
- (4) Considering storage capacity and permeability as standard, the pore structure of the Xiagou Formation tight oil reservoir was categorized into three types. The type I pore structure features a movable fluid saturation of more than 20% and a permeability of more than 0.1 mD. Dissolving and microfracture development significantly enhance the size and connection of pore-throats. Movable fluid saturation of type II pore structures is between 10% and 20%, and permeability is generally between 0.05 and 0.1 mD. Dissolution is weak, few microfractures are developed, and common clay mineral filling occurs, reducing the pore space. Movable fluid saturation of the type III pore structure measures less than 10%, and permeability is basically below 0.05 mD. Strong development of clay mineral filling inhibits fluid flow, notably reducing mobile fluid saturation of the tight oil reservoir. Therefore, the type I pore structure with high permeability, large ratio of macropores, and medium pore-throat allocation presents the best pore-throat configuration, a large reservoir performance, and strong permeating ability. Therefore, the type I pore structure reservoir should be regarded as a key area for surveying of the tight oil reservoir “sweet spots” in the study area

Data Availability

The data that support the findings of this study are available from the corresponding author upon reasonable request.

Conflicts of Interest

There are no conflicts of interest with respect to the results of this paper.

Acknowledgments

We thank PetroChina Yumen Oilfield Company for providing samples and data access. This work was financially supported by the Natural Science Foundation of Hebei

Province for Youth (D2019403189) and the National Natural Science Foundation of China (Grant No. 41372145), and we thank the sponsors of these projects.

References

- [1] X. X. Wang, J. G. Hou, S. H. Li et al., “Insight into the nano-scale pore structure of organic-rich shales in the Bakken Formation, USA,” *Journal of Petroleum Science and Engineering*, vol. 191, article 107182, 2020.
- [2] J. Qiao, A. Baniasad, L. Zieger, C. Zhang, Q. Luo, and R. Littke, “Paleo-depositional environment, origin and characteristics of organic matter of the Triassic Chang 7 Member of the Yanchang Formation throughout the mid-western part of the Ordos Basin, China,” *International Journal of Coal Geology*, vol. 237, p. 103636, 2021.
- [3] B. E. Law and J. B. Curtis, “Introduction to unconventional petroleum systems,” *AAPG Bulletin*, vol. 86, no. 11, pp. 1851–1852, 2002.
- [4] K. E. Higgs, H. Zwingmann, A. G. Reyes, and R. H. Funnell, “Diagenesis, porosity evolution and petroleum emplacement in tight gas reservoirs, Taranaki Basin, New Zealand,” *Journal of Sedimentary Research*, vol. 77, no. 12, pp. 1003–1025, 2007.
- [5] S. H. Lin, C. N. Zou, and X. J. Yuan, “Status quo of tight oil exploitation in the United States and its implication,” *Lithologic Reservoirs*, vol. 23, no. 4, pp. 25–30, 2011.
- [6] H. Gao and H. A. Li, “Pore structure characterization, permeability evaluation and enhanced gas recovery techniques of tight gas sandstones,” *Journal of Natural Gas Science and Engineering*, vol. 28, pp. 536–547, 2016.
- [7] Q. Chen, Y. Deng, J. Wei et al., “Types, distribution and play targets of Lower Cretaceous tight oil in Jiuquan Basin, NW China,” *Petroleum Exploration and Development*, vol. 45, no. 2, pp. 227–238, 2018.
- [8] C. Jia, C. Zou, J. Li, D. Li, and M. Zheng, “Assessment criteria, main types, basic features and resource prospects of the tight oil in China,” *Acta Petrolei Sinica*, vol. 33, no. 3, pp. 343–350, 2012.
- [9] H. G. Wen, R. C. Zheng, and T. R. Ye, “Sedimentary characteristics of the Lower Cretaceous strata and prediction of the favourable exploration areas in the Qingxi depression, Jiuxi Basin, Gansu,” *Sedimentary Geology and Tethyan Geology*, vol. 4, pp. 71–77, 2005.
- [10] C. Zou, R. Zhu, and S. Wu, “Types, characteristics, genesis and prospects of conventional and unconventional hydrocarbon accumulations: taking tight oil and tight gas as an instance,” *Acta Petrolei Sinica*, vol. 33, no. 2, pp. 173–187, 2012.
- [11] B. Gao, “Analysis of thermal evolution and hydrocarbon-generating history of source rocks in Qingnan sub-sag in Jiuxi depression,” *Oil & Gas Geology*, vol. 25, no. 3, pp. 288–293, 2004.
- [12] Q. Luo, C. Zhang, Q. Dai et al., “Characterization of compact carbonate pore-throat network systems in the Xiagou Formation in Qingxi Sag, Jiuquan Basin, China,” *Journal of Petroleum Science and Engineering*, vol. 159, pp. 853–868, 2017.
- [13] C. Zou, *Unconventional petroleum geology*, pp. 363–373, Petroleum Industry Press, 2012.
- [14] C. Zou, Z. Yang, S. Tao et al., “Nano-hydrocarbon and the accumulation in coexisting source and reservoir,” *Petroleum Exploration and Development*, vol. 39, no. 1, pp. 15–32, 2012.

- [15] Z. Wang, "Research progress, existing problem and development trend of tight rock oil," *Petroleum Geology & Experiment*, vol. 35, no. 6, 2013.
- [16] J. Du, H. Liu, D. Ma, J. Fu, Y. Wang, and T. Zhou, "Discussion on effective development techniques for continental tight oil in China," *Petroleum Exploration and Development*, vol. 41, no. 2, pp. 217–224, 2014.
- [17] C. Jia, M. Zheng, and Y. Zhang, "Unconventional hydrocarbon resources in China and the prospect of exploration and development," *Petroleum Exploration and Development*, vol. 39, no. 2, pp. 129–135, 2012.
- [18] R. Zheng, C. Wang, L. Zhu, H. Liu, and G. Fang, "Discovery of the first example of "white smoke type" of exhalative rock (hydrothermal sedimentary dolostone) in Jiuxi basin and its significance," *Journal of Chengdu University of Technology*, vol. 30, no. 1, pp. 1–8, 2003.
- [19] J. Chen, J. Chen, L. Zhang, and N. Zhong, "New understandings on hydrocarbon and exploration direction in Jiuxi basin," *Petroleum Exploration and Development*, vol. 1, pp. 19–22, 2001.
- [20] C. L. Perrin, P. M. Tardy, K. S. Sorbie, and J. C. Crawshaw, "Experimental and modeling study of Newtonian and non-Newtonian fluid flow in pore network micromodels," *Journal of Colloid and Interface Science*, vol. 295, no. 2, pp. 542–550, 2006.
- [21] B. Christian, A. Cattaneo, and M. Szuman, "Sedimentary structures offshore Ortona, Adriatic Sea—deformation or sediment waves," *Marine Geology*, vol. 234, no. 1–4, pp. 261–270, 2006.
- [22] R. G. Loucks, M. R. Reed, S. C. Ruppel, and U. Hammes, "Spectrum of pore types and networks in mudrocks and a descriptive classification for matrix-related mudrock pores," *AAPG Bulletin*, vol. 96, no. 6, pp. 1071–1098, 2012.
- [23] W. Yang, Q. Wang, Y. Wang et al., "Pore characteristic responses to categories of depositional microfacies of delta-lacustrine tight reservoirs in the Upper Triassic Yanchang Formation, Ordos Basin, NW China," *Marine and Petroleum Geology*, vol. 118, article 104423, 2020.
- [24] B. Annapurna and S. Ganapathi, "Microstructure and pore system analysis of Barren Measures shale of Raniganj field, India," *Journal of Natural Gas Science and Engineering*, vol. 26, pp. 427–437, 2015.
- [25] G. Stéphane, J. C. Robinet, and D. Prêt, "Optimization of pore-network characterization of a compacted clay material by TEM and FIB/SEM imaging," *Microporous & Mesoporous Materials*, vol. 224, pp. 116–128, 2016.
- [26] S. Chen, H. Wang, J. Wei, Z. Y. Lv, H. J. Gan, and S. D. Jin, "Sedimentation of the lower cretaceous Xiagou Formation and its response to regional tectonics in the Qingxi Sag, Jiuquan Basin, NW China," *Cretaceous Research*, vol. 47, pp. 72–86, 2014.
- [27] M. Z. Zhang, L. M. Ji, B. du, S. Dai, and X. W. Hou, "Palynology of the Early Cretaceous Hanxia Section in the Jiuquan Basin, Northwest China: the discovery of diverse early angiosperm pollen and paleoclimatic significance," *Palaeogeography, Palaeoclimatology, Palaeoecology*, vol. 440, no. 15, pp. 297–306, 2015.
- [28] S. Li, Q. F. Wang, and H. C. Zhang, "Charophytes from the lower Cretaceous Xiagou formation in the Jiuquan basin (northwestern China) and their palaeogeographical significance," *Cretaceous Research*, vol. 105, article 103940, 2020.
- [29] W. Ju and W. F. Sun, "Tectonic fractures in the Lower Cretaceous Xiagou Formation of Qingxi Oilfield, Jiuxi Basin, NW China. Part two: numerical simulation of tectonic stress field and prediction of tectonic fractures," *Journal of Petroleum Science and Engineering*, vol. 146, pp. 626–636, 2016.
- [30] P. Jin, L. Ji, B. Ma, B. Yuan, and L. Long, "Early Cretaceous palynology and paleoclimate of the Hanxia-Hongliuxia area, Jiuxi basin, China," *Review of Palaeobotany and Palynology*, vol. 281, article 104259, 2020.
- [31] W. Ju, Z. L. Li, W. F. Sun, and H. R. Xu, "In-situ stress orientations in the Xiagou tight oil reservoir of Qingxi Oilfield, Jiuxi Basin, northwestern China," *Marine and Petroleum Geology*, vol. 98, pp. 258–269, 2018.
- [32] Y. C. Guo, Y. Song, X. X. Fang, X. Pang, and T. Li, "Reservoir characterization of an organic-rich dolomitic tight-oil reservoir, the Lower Cretaceous Xiagou Formation in the Qingxi sag, Jiuquan basin, NW China," *Marine and Petroleum Geology*, vol. 89, no. 3, pp. 541–559, 2018.
- [33] Y. Zhao, X. Zhou, C. Wang, M. F. Wang, and J. J. Guo, "Characters of a special rock-fractured reservoir and factors of controlling fractured development at Qingxi Oilfield in Jiuxi Basin," *Natural Gas Geoscience*, vol. 16, no. 1, pp. 12–15, 2005.
- [34] B. Q. Wang, H. L. Chen, S. F. Yang, A. C. Xiao, X. Cheng, and J. A. Rupp, "Geometry and kinematics of Late Cretaceous inversion structures in the Jiuquan Basin, western China," *Cretaceous Research*, vol. 26, no. 2, pp. 319–327, 2005.
- [35] S. J. Vincent and M. B. Allen, "Evolution of the Minle and Chaoshui Basins, China: implications for Mesozoic strike-slip basin formation in Central Asia," *Geological Society of America Bulletin*, vol. 111, no. 5, pp. 725–742, 1999.
- [36] P. Luo, S. Yang, L. Ma, and L. Su, "Originization, characteristics and exploration significance of meso-plagioclase in lacustrine layered muddy dolomite in Qingxi Depression, Liuxi Basin," *Petroleum Exploration and Development*, vol. 28, no. 6, pp. 32–33, 2001.
- [37] W. Yan, X. Zhu, L. Gu, Q. Zhang, Z. Zhang, and X. Wang, "Fractures in the Lower Cretaceous reservoir of Qingxi Oilfield, Jiuxi Depression, Northwest China," *Petroleum Exploration and Development*, vol. 31, no. 1, pp. 54–56, 2004.
- [38] J. P. Su, B. X. Wu, and H. Y. Lei, "The sedimentary formation and analyses for dynamic evolution of Jiuxi Cretaceous Basin, Gansu Province," *Acta Sedimentologica Sinica*, vol. 20, no. 4, pp. 568–573, 2002.
- [39] J. Chen, W. Zhao, D. Huang, C. Zou, Z. Wang, and J. Chen, "Differences and similarities and exploration of oil and gas in Jiu Dong and Jiu Xi basin," *Petroleum Exploration and Development*, vol. 24, no. 6, pp. 12–16, 1997.
- [40] S. D. Jin, H. Y. Cao, and H. Wang, "Orbital cyclicity in sedimentary sequence and climatic indications of C-O isotopes from lower cretaceous in Qingxi sag, Jiuquan basin, NW China," *Geoscience Frontiers*, vol. 10, no. 2, pp. 112–124, 2019.
- [41] Q. Wang, Y. Li, W. Yang et al., "Finite element simulation of multi-scale bedding fractures in tight sandstone oil reservoir," *Energies*, vol. 13, no. 1, p. 131, 2019.
- [42] A. Wang, Y. Wei, Y. Yuan, C. Li, Y. Li, and D. Cao, "Coalbed methane reservoirs' pore-structure characterization of different macrolithotypes in the southern Junggar Basin of Northwest China," *Marine and Petroleum Geology*, vol. 86, pp. 675–688, 2017.
- [43] X. Liu, J. Zhang, Y. Bai, Y. Zhang, and J. Liu, "Pore structure petrophysical characterization of the upper cretaceous oil shale from the Songliao basin (NE China) using low-field NMR," *Journal of Spectroscopy*, vol. 5, no. 1–11, 2020.

- [44] M. Pilotti, "Reconstruction of clastic porous media," *Transport in Porous Media*, vol. 41, no. 3, pp. 359–364, 2000.
- [45] O. Lame, D. Bellet, M. di Michiel, and D. Bouvard, "Bulk observation of metal powder sintering by X-ray synchrotron microtomography," *Acta Materialia*, vol. 52, no. 4, pp. 977–984, 2004.
- [46] D. Attwood, "Nanotomography comes of age," *Nature*, vol. 442, no. 7103, pp. 642–643, 2006.
- [47] A. Sakdinawat and D. Attwood, "Nanoscale X-ray imaging," *Nature Photonics*, vol. 4, no. 12, pp. 840–848, 2010.
- [48] A. Sufian and A. R. Russell, "Microstructural pore changes and energy dissipation in Gosford sandstone during pre-failure loading using X-ray CT," *International Journal of Rock Mechanics and Mining Sciences*, vol. 57, pp. 119–131, 2013.
- [49] K. Zhang, C. Z. Jia, Y. Song et al., "Analysis of Lower Cambrian shale gas composition, source and accumulation pattern in different tectonic backgrounds: a case study of Weiyuan Block in the Upper Yangtze region and Xiuyu Basin in the Lower Yangtze region," *Fuel*, vol. 263, article 115978, 2020.
- [50] F. Peng, D. K. Luo, C. F. Yin, C. Wang, and P. Shirish, "Tight oil accumulation characteristics and resource potential evaluation of the Xiagou formation in Qingxi depression, Jiuquan basin," *Energy Procedia*, vol. 158, pp. 5940–5945, 2019.
- [51] S. Hu, W. Zhao, L. Hou et al., "Development potential and technical strategy of continental shale oil in China," *Petroleum Exploration and Development*, vol. 47, no. 4, pp. 877–887, 2020.
- [52] G. He, *Reservoir physics*, Petroleum Industry Press, Beijing, 1994.
- [53] Y. Ji, *Oil and gas reservoir geology*, China University of Petroleum Press, Dongying, 2009.
- [54] W. Zhao, C. Jia, L. Jiang et al., "Fluid charging and hydrocarbon accumulation in the sweet spot, Ordos Basin, China," *Journal of Petroleum Science and Engineering*, vol. 200, article 108391, 2021.
- [55] G. M. Wang, R. Zhu, X. Y. Zheng, J. Hu, Z. Wang, and X. M. Shi, "Characterization and genetic significance of mold pores in tight sandstone: A case from the lower part of the Yanchang Formation in the Wuqi-Ansai area," *Marine and Petroleum Geology*, vol. 124, article 104790, 2021.
- [56] A. Mehmami, R. Verma, and M. Prodanović, "Pore-scale modeling of carbonates," *Marine and Petroleum Geology*, vol. 114, article 104141, 2020.
- [57] S. Zhu, H. Cui, Y. Jia, X. Zhu, H. Tong, and L. Ma, "Occurrence, composition, and origin of analcime in sedimentary rocks of non-marine petroliferous basins in China," *Marine and Petroleum Geology*, vol. 113, article 104164, 2020.
- [58] I. Armenteros, "Chapter 2 Diagenesis of Carbonates in Continental Settings," *Developments in Sedimentology*, pp. 61–151, 2010.
- [59] A. C. Azerêdo, N. Inês, and P. Bizarro, "Carbonate reservoir outcrop analogues with a glance at pore-scale (middle Jurassic, Lusitanian basin, Portugal)," *Marine and Petroleum Geology*, vol. 111, pp. 815–851, 2020.
- [60] C. Jacquemyn, H. el Desouky, D. Hunt, G. Casini, and R. Swennen, "Dolomitization of the Latemar platform: fluid flow and dolomite evolution," *Marine and Petroleum Geology*, vol. 55, pp. 43–67, 2014.
- [61] T. Dong, Q. He, S. He et al., "Quartz types, origins and organic matter-hosted pore systems in the lower Cambrian Niutitang formation, middle Yangtze platform, China," *Marine and Petroleum Geology*, vol. 123, article 104739, 2020.
- [62] Q. Dai, Q. Luo, C. Zhang et al., "Pore structure characteristics of tight-oil sandstone reservoir based on a new parameter measured by NMR experiment: a case study of seventh member in Yanchang Formation, Ordos Basin," *Acta Petrolei Sinica*, vol. 7, pp. 887–897, 2016.
- [63] J. Zhao, Z. Liu, Q. Xie, and Z. Jingping, "Micro pore-throat structural classification of Chang 7 tight oil reservoir of Jiyuan Oilfield in Ordos Basin," *China Petroleum Exploration*, vol. 19, no. 5, pp. 73–79, 2014.
- [64] S. Wu, Z. Cai, and S. Shi, *Oil geology*, Petroleum Industry Press, Beijing, 2011.
- [65] C. Xin, Y. He, and G. Dong, "The application of the capillary pressure curve in micro-cosmic reservoir heterogeneity," *Henan petroleum*, vol. 20, no. 3, pp. 57–59, 2006.